Radio Interferometric Studies of Cool Evolved Stellar Winds

A dissertation submitted to the University of Dublin
for the degree of Doctor of Philosophy

Eamon O'Gorman

Supervisor: Dr. Graham M. Harper

Trinity College Dublin, September 2013

School of Physics
University of Dublin
Trinity College

Declaration

I declare that this thesis has not been submitted as an exercise for a degree at this or any other university and it is entirely my own work.

I agree to deposit this thesis in the University's open access institutional repository or allow the library to do so on my behalf, subject to Irish Copyright Legislation and Trinity College Library conditions of use and acknowledgement.

Name: Eamon O'Gorman

Signature: ..... **Date:** .....

Summary

You should write a nice summary here...

For Mum and Dad,
a constant source of inspiration and guidance.

Acknowledgements

Some sincere acknowledgements...

List of Publications

Refereed

1. **O'Gorman, E.**, Harper, G. M., Brown, A., Brown, A., Drake, S., and Richards, A. M. S.
   "Multi-wavelength Radio Continuum Emission Studies of Dust-free Red Giants"
   The Astronomical Journal, 146, 98, (2013)

2. Richards, A. M. S., Davis, R. J., Decin, L., Etoka, S., Harper, G. M., Lim, J. J., Garrington, S. T., Gray, M. D., McDonald, I., **O'Gorman, E.**, Wittkowski, M.
   "e-MERLIN resolves Betelgeuse at wavelength 5 cm"
   Monthly Notices of the Royal Astronomical Society Letters, 432, L61 (2013)

3. **O'Gorman, E.**, Harper, G. M., Brown, J. M., Brown, A., Redfield, S., Richter, M. J., and Requena-Torres, M. A.
   "CARMA CO(J = 2 - 1) Observations of the Circumstellar Envelope of Betelgeuse"
   The Astronomical Journal, 144, 36 (2012)

4. Sada, P. V., Deming, D., Jennings, D. E., Jackson, B. K., Hamilton, C. M., Fraine, J., Peterson, S. W., Haase, F., Bays, K., Lunsford, A., and **O'Gorman, E.**
   "Extrasolar Planet Transits Observed at Kitt Peak National Observatory"
   Publications of the Astronomical Society of the Pacific, 124, 212 (2012)

5. Sada, P. V., Deming, D., Jackson, B. K., Jennings, D. E., Peterson, S. W., Haase, F., Bays, K., **O'Gorman, E.**, and Lundsford, A.
"Recent Transits of the Super-Earth Exoplanet GJ 1214b"
The Astrophysical Journal Letters, 720, L215 (2010)

Non-Refereed

1. **O'Gorman, E.**, & Harper, G. M.
"What is Heating Arcturus' Wind?",
Proceedings of the 16th Cambridge Workshop on Cool Stars, Stellar Systems and the Sun. Astronomical Society of the Pacific Conference Series, 448, 691 (2011)

Contents

List of Publications vi

List of Figures x

List of Tables xi

1 Introduction 1

1.1 Motivation for Researching Cool Evolved Stellar Winds 2
1.2 On the Nature of Cool Evolved Stellar Atmospheres 4
1.3 Basic Concepts of Stellar Winds 8
1.4 Stellar Wind Driving Mechanisms Across the H-R Diagram 10
1.4.1 Radiatively Driven Winds 11
1.4.2 Solar Type Winds 12
1.4.3 Cool Evolved Stellar Winds 13
1.5 Red Giant and Red Supergiant Evolution 15
1.5.1 Change in Atmospheric Dynamics 15
1.5.2 Evolutionary Tracks 16
1.6 Radio Emission from Stellar Atmospheres 20
1.7 Radio Emission Mechanisms 22
1.7.1 Thermal Free-free (Bremsstrahlung) Emission 23
1.7.2 Molecular Line Emission 24
1.8 Radio Observations of Stellar Atmospheres 26
1.8.1 Brightness Temperature 26
1.8.2 Brightness Temperature and Flux Density 28
1.8.3 Thermal Free-free Radio Opacity 29
1.8.4 Radio Excess from Stellar Winds 32

1.8.5 Molecular Emission Lines from Stellar Winds 35
1.9 Outline and Goals of this Thesis 37

A List of Abbreviations Used in this Thesis. **38**

B Discrete Absorption Feature **40**

References **42**

List of Figures

1.1 The Linsky-Haisch dividing line. 5
1.3 Stellar winds across the H-R diagram. 11
1.4 Evolutionary tracks of massive stars. 17
1.5 Evolution track of an intermediate mass star. 18
1.6 Radio H-R diagram. 21
1.7 Molecular ladder plot and relative populations. 25
1.11 Theoretical molecular line profiles. 36

List of Tables

1.1 Properties of main sequence and evolved stars 16

A.1 List of Abbreviations 38

1 Introduction

This chapter begins with outlining the motivation for studying winds from cool evolved stars while simultaneously highlighting the problems associated their mass-loss mechanisms. The fundamental physics governing these winds along with their physical properties are then discussed in detail. Their mass outflows are subsequently compared with other types of stars across the Hertzsprung Russel diagram and a description of how stars evolve to become red giants and red supergiants in also included. The second half of this chapter focuses on radio emission from stellar winds. The radio emission mechanisms that are relevant to this thesis are discussed and the terminology required to study cool evolved stellar winds at radio wavelengths is introduced. This chapter concludes with a brief outline of the remaining chapters within this thesis.

1.1 Motivation for Researching Cool Evolved Stellar Winds

Mass-loss from non-coronal spectral-type K through mid-M evolved stars plays a crucial role in galactic evolution and ultimately provides part of the material required for the next generation of stars and planets. This mass-loss occurs via a cool ($T_e \lesssim 10^4\,K$) wind with terminal velocities typically less than the photospheric escape velocity ($10 \leq v_\infty \leq 50\,\mathrm{km\,s^{-1}}$). The mass-loss rates for the red giants are significant, typically $10^{-11} - 10^{-9}\,M_\odot\,\mathrm{yr}^{-1}$, and are even higher for the more short-lived red supergiants, typically $10^{-6} - 10^{-4}\,M_\odot\,\mathrm{yr}^{-1}$. This implies that a substantial fraction of the star's initial mass can be dispersed to the interstellar medium (ISM) during these post main sequence evolutionary stages (e.g., Schröder & Sedlmayr, 2001). Mass-loss from these stars is therefore a crucial factor governing stellar evolution (Chiosi & Maeder, 1986), and also in explaining the frequency of supernovae in the galaxy (Dohm-Palmer & Skillman, 2002; van Loon, 2010). Despite the importance of this phenomenon, and decades of study, the mechanisms that drive winds from evolved spectral-type K through mid-M stars remain unknown (clearly laid out by Holzer & MacGregor 1985 but still unsolved, e.g., Crowley *et al.* 2009). There is insufficient atomic, molecular, or dust opacity to drive a radiation-driven outflow (Jones, 2008; Zuckerman *et al.*, 1995) and acoustic/pulsation models cannot drive the observed mass-loss rates (Sutmann & Cuntz, 1995). Ultraviolet (UV) and optical observations reveal an absence of significant hot wind plasma, and the winds are thus too cool to be Parker-type thermally-driven flows (e.g., Ayres *et al.*, 1981; Haisch *et al.*, 1980; Linsky & Haisch, 1979).

Magnetic fields are most likely involved in the mass-loss process, although current magnetic models are also unable to explain spectral diagnostics. Exquisite high signal-to-noise ratio (S/N) *Hubble Space Telescope* (HST) UV spectra have revealed that the 1-D linear Alfvén wave-driven wind models of the 1980s (e.g., Harper 1988; Hartmann & MacGregor 1980) are untenable (Harper *et al.*, 2001). These models predict chromospheres as integral parts of a turbulent, extended, and heated wind acceleration zone, but the theoretical line profiles and electron densities do not agree with the *HST* spectra, (e.g., Judge & Carpenter, 1998).

A new generation of theoretical models with outflows driven within diverging magnetic flux tubes have now emerged (Falceta-Gonçalves *et al.*, 2006; Suzuki, 2007) but these too are not yet in agreement with observations (Crowley *et al.*, 2009). It has also been suggested that the winds may be driven by some form of magnetic pressure acting on very highly clumped wind material (Eaton, 2008) but Harper (2010) does not find compelling evidence for this hypothesis. Progress in this field continues to be driven by observations which can test existing models and theories, and provide new insights and constraints into the mass-loss problem.

The Advantages of Radio Observations

Understanding the dynamics and thermodynamics of the atmospheres of late-type evolved stars will ultimately lead to a broader understanding of their mass-loss processes. Red supergiants have extended atmospheres which contain a mixture of atoms, ions, molecules, and dust, and are an ideal test bed for ideas and theories of mass-loss. These atmospheres are so extended that the closest red supergiants can be spatially resolved and imaged at centimeter and millimeter-wavelengths, both in continuum and molecular line emission. Such observations can yield direct measurements of the gas temperature, velocity, and atmospheric structure, which can be used to provide essential constraints on the mass-loss process. The red giants[1] on the other hand have less extended atmospheres which are dust free and contain only small abundances of molecules. They currently[2] cannot be spatially resolved at radio wavelengths, but their partially ionized outflows can still be detected at these wavelengths, providing an area-averaged sweep through the atmospheres of these stars. The lack of spatial resolution prevents the direct measurement of the fundamental atmospheric properties. However, point source radio observations can still be compared against existing atmospheric models based on shorter wavelength observations (e.g., models based on optical and UV observations). Such radio observations sample further out in the star's atmosphere than optical and UV observations and can test the validity of and improve upon existing model atmospheres.

[1] The term *red giant* excludes asymptotic giant branch stars throughout this thesis.

[2] ALMA and e-MERLIN will eventually be capable of spatially resolving the atmospheres of red giants.

1.2 On the Nature of Cool Evolved Stellar Atmospheres

The study of stellar outflows from cool evolved stars began with the discovery of blue-shifted absorption features (i.e., "P Cygni type" profiles) in strong resonance lines from a number of bright red supergiants (Adams & MacCormack, 1935). They attributed these features to gradually expanding envelopes, even though the expansion speed velocity was small ($\sim 5\,\mathrm{km\,s^{-1}}$) and much less than the photospheric escape velocity. Spitzer (1939) analyzed similar data and devised a *fountain model* for the atmospheres of red supergiants. In this model, radiation drives matter upwards from the photosphere until at some height, the ionization state of the matter changes, causing the radiation force to drop so that the matter falls back onto the star. Definitive evidence for mass-loss from cool evolved stars came from Deutsch (1956) who observed a system which contained an M5 giant (i.e., α Her) and a G5 dwarf. They found that the same blue-shifted absorption features were present in the spectrum of both stars, which were not present in other single G5 stars. This indicated that both stars were enveloped in material which had been emitted from the M5 giant. The inferred expansion velocity at the distance of the G5 dwarf was sufficient to escape the system, thus confirming that matter was escaping the gravitational potential of the α Her system.

Even though many later studies concluded that evolved late-type stars contained cool ($T_e < 1000\,\mathrm{K}$) extended circumstellar environments (e.g., Bernat & Lambert, 1976; Gehrz & Woolf, 1971; Reimers, 1975; Weymann, 1962), the physical properties of the ouflow between the photosphere and this cool outer environment remained unclear. An important discovery in late-type evolved stellar atmospheres resulted from the first ultraviolet survey of such stars using the *International Ultraviolet Explorer* (IUE; Macchetto & Penston, 1978). The survey revealed a "transition region dividing line" in the giant branch near spectral type K1 and in the supergiant branch near spectral type G5, which separates these stars based on the properties of their atmospheres (Linsky & Haisch, 1979; Simon *et al.*, 1982). In Figure 1.1 we show the approximate location of this dividing line in the H-R diagram. Stars blueward of the dividing line were found to possess chromospheres and transition regions like the Sun, while stars on the red side were

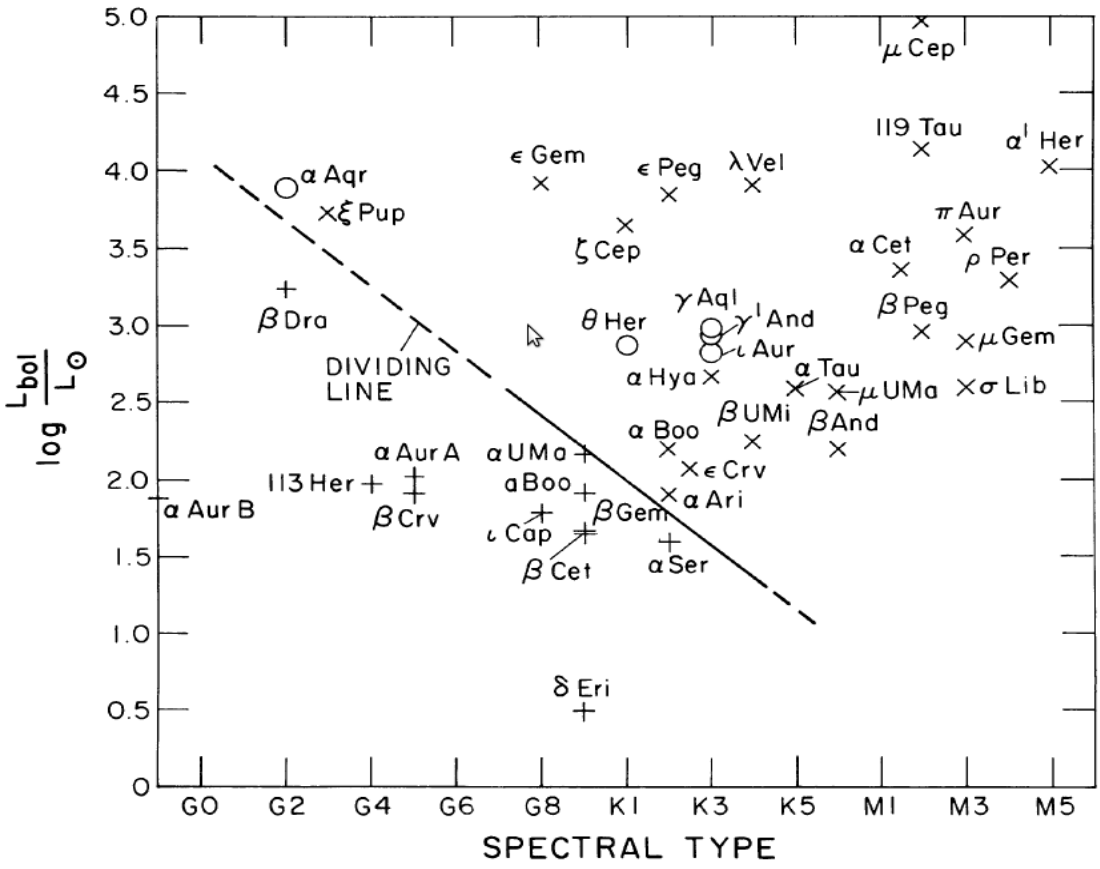

Figure 1.1: A section of the H-R diagram showing the Linsky-Haisch dividing line which was proposed as a sharp division separating coronal (indicated by plus signs) from non-coronal (indicated by crosses) evolved late-type stars. Hybrid atmosphere stars are marked by circles. This image is taken from Drake & Linsky (1986) who carried out a 6 cm survey of late-type evolved stars.

found to possess chromospheres and cool winds. X-ray observations showed that this dividing line extended to coronal emission (Ayres *et al.*, 1981). Around the same time, another class of late-type evolved star emerged which showed signs of possessing both a transition region and a cool wind (e.g., Reimers, 1982). Many of these so-called "hybrid atmosphere" stars now also show evidence for coronal emission, albeit much weaker than on the blue side of the dividing line (Ayres *et al.*, 1997; Dupree *et al.*, 2005).

Following the advent of *HST*, the important UV diagnostic transitions (e.g.,

lines from C II, Fe II, Mg II, and O II) could be observed with exquisite detail. The photon-scattering wind produces self-reversals in these chromospheric emission lines and have revealed that, for the most part, the red giant winds accelerate in a quasi-steady manner and are not the result of ballistic ejecta. This is inferred by the increase of wind scattering absorption velocity with optical depth, and thus height in the wind, as shown in Figure 1.2 for λ Vel (Carpenter *et al.*, 1999). The P Cygni-type line profiles, which are indicative of stellar outflows,

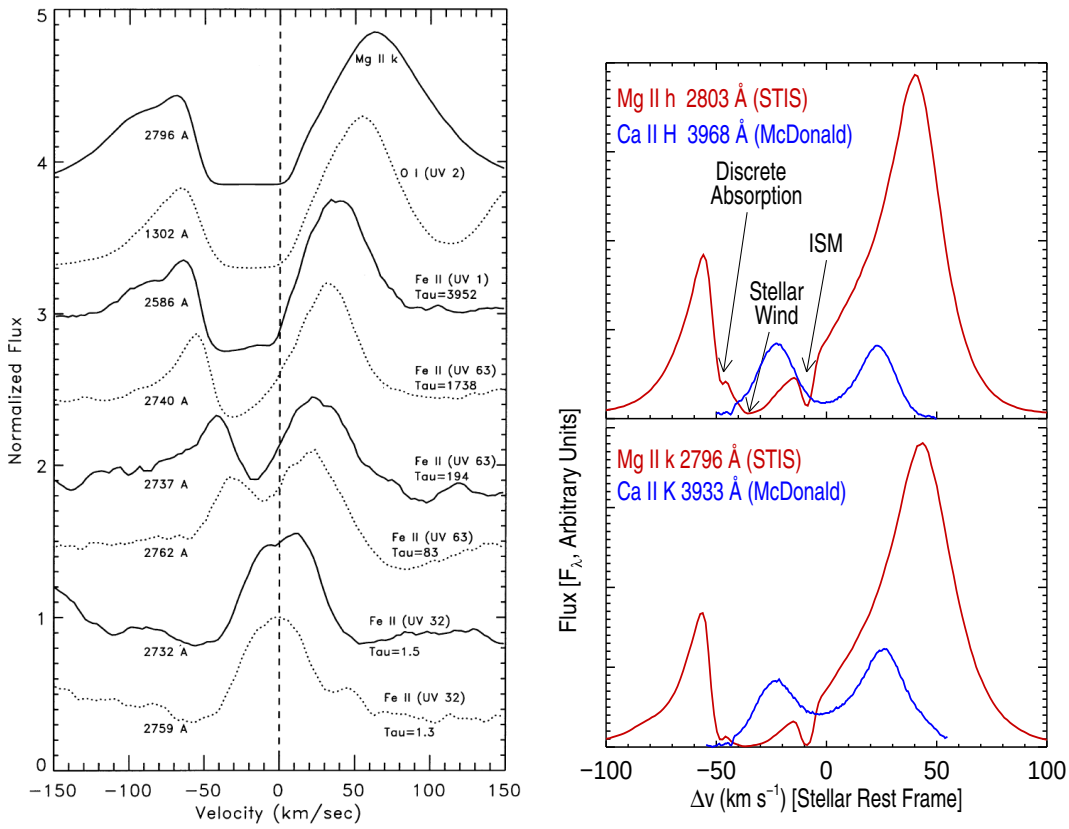

Figure 1.2: *Left: HST* Goddard High-Resolution Spectrograph (GHRS) spectra showing the increase of wind scattering absorption velocity with optical depth for strong chromospheric lines. These data were taken for λ Vel (a K5 Ib-II star) and show that it's wind accelerates in a quasi-steady manner. *Right:* The Mg II *h* and *k* and Ca II H and K line profiles of α Boo. For many cool evolved stars, these strong resonant lines have often been compared to synthetic profiles to provide estimates of atmospheric properties. Three absorption components are present in the high S/N *HST* data and originate from the ISM, the stellar wind, and an unknown source (See Appendix B).

are also shown in Figure 1.2 for the Mg II and Ca II resonance lines of α Boo (K2 III). For many evolved stars, these disk averaged emission line profiles have also provided crude estimates of atmospheric properties such as the mass-loss rate and terminal velocity, by comparing them to synthetic profiles based on detailed radiative transfer code (e.g., Robinson *et al.*, 1998).

Chromospheres are the manifestation of surface convection and are found almost exclusively in the cool portion of the H-R diagram (Ayres, 2010a). These non-radiatively heated regions of the inner atmosphere are present in the atmospheres of all late-type evolved stars. The density scale height, H_ρ, is the height in the atmosphere where the density drops by a factor of e^{-1} and is defined as

$$H_\rho = \frac{kT_e R_\star^2}{GM_\star}. \tag{1.1}$$

Here, k is Boltzmann's constant, T_e is the electron temperature, $R_\star$ is the stellar radius, G is the gravitational constant, and $M_\star$ is the stellar mass. The much larger radii of evolved stars means that their *typical* scale height is over two orders of magnitude greater than that of the Sun. It is for this reason that their chromospheres are believed to be much more extended than the Sun's. The red supergiants are now known to have chromospheres which extend out to a few $R_\star$ (Harper *et al.*, 2001; Lim *et al.*, 1998). However, there is still much debate regarding the spatial extent of chromospheres in red giants. Carpenter *et al.* (1985) used measurements of the total emission-line flux and line ratios within the C II multiplet to conclude that coronal giants had thin chromospheres ($\lesssim 0.1\,R_\star$) while the chromospheres in the non-coronal giants were much more extended ($\sim 2.5\,R_\star$). Recently, Berio *et al.* (2011) found that β Ceti, a coronal giant, has a chromosphere which may extend out to $\sim 1.5\,R_\star$, while Luttermoser *et al.* (1994) finds that the chromospheric spatial extend of an M6 giant to be $\leq 1.05\,R_\star$. These findings are in conflict with one another and it is apparent that the spatial extent of the chromosphere in red giants is currently uncertain.

1.3 Basic Concepts of Stellar Winds

The addition of energy above the photosphere is a requirement for a stellar outflow to escape the gravitational potential of a star. This energy input can be either in the form of a heat input (e.g., ambipolar diffusion heating), or in the form of a momentum input (e.g., radiation pressure on gas species). The momentum input is described by Newton's second law, $F = dp/dt$, where F is the outward force and p is the momentum. For this reason, the presence of an outward force is usually called momentum deposition, in contrast to energy deposition. The momentum deposition is governed by the momentum equation

$$F = \rho d\boldsymbol{v}/dt \tag{1.2}$$

where ρ is the mass density, and $\boldsymbol{v}$ is the velocity vector. In spherical symmetry, the velocity gradient is

$$\frac{dv(r,t)}{dt} = \frac{\partial v(r,t)}{\partial t} + \frac{\partial v(r,t)}{\partial r}\frac{dr(t)}{dt} = v\frac{dv}{dr}, \tag{1.3}$$

where we have assumed a stationary flow. The momentum equation for a flow being acted on by an outward directed force per unit mass, $f = f(r)$, is then

$$v\frac{dv}{dr} = -\frac{1}{\rho}\frac{dP}{dr} - \frac{GM_\star}{r^2} + f \tag{1.4}$$

where each of these terms have units of $\mathrm{cm\,s^{-2}}$ (e.g., Lamers & Cassinelli, 1999). The term on to the left of Equation 1.4 is the acceleration, which is produced by the gas pressure gradient (first term on right), the gravity (second term on right), and some other force(s) which are contained in f. The gas pressure gradient term is directed outwards (positive) because $dP/dr < 0$.

The gas pressure gradient in Equation 1.4 depends on the temperature structure of the outflow, which in turn depends on the heating and cooling. The effects of energy deposition can be expressed via the first law of thermodynamics

$$\frac{du}{dt} = \frac{dq}{dt} - P\left(\frac{d\rho^{-1}}{dt}\right) \tag{1.5}$$

where $u = (3/2)(\mathcal{R}T/\mu)$ is the internal energy of the system per unit mass, q is

the net heat gained per unit mass, and the final term is the work done by the gas per unit time per unit mass. The time dependence can be removed using $d/dt = v\, d/dr$ to give

$$\frac{dq}{dr} = \frac{3}{2}\frac{\mathcal{R}}{\mu}\frac{dT}{dr} + P\frac{d\rho^{-1}}{dr}. \tag{1.6}$$

The ideal gas law can be written as

$$\rho = \frac{\mu P}{\mathcal{R}T}, \tag{1.7}$$

and substituting this into the last term in Equation 1.6 gives the desired expression which relates the gas pressure to the heating:

$$\frac{1}{\rho}\frac{dP}{dr} = \frac{5}{2}\frac{\mathcal{R}}{\mu}\frac{dT}{dr} - \frac{dq}{dr}. \tag{1.8}$$

The energy equation for stellar outflows can then be found by replacing the gas pressure term in the momentum equation with an expression which depends on the temperature structure of the outflow and the heating, i.e., combining Equations 1.4 and 1.8:

$$\frac{d}{dr}\left(\frac{v^2}{2} + \frac{5\mathcal{R}T}{2\mu} - \frac{GM_\star}{r}\right) = f(r) + \frac{dq}{dr}. \tag{1.9}$$

The combination of the terms inside the brackets on the left gives the total energy of the system per unit mass, with the first term being the kinetic energy of the flow, the second term being the enthalpy of the gas (the internal kinetic energy plus the capacity to do work), and the third term being the gravitational potential energy. This equation tells us that the change in total energy of the gas as it moves a unit distance outwards from the star, is equal to the momentum input by the force and the heat input.

The energy equation in the form of Equation 1.9 is called the *Bernoulli* equation. Integrating the Bernoulli equation gives

$$\begin{aligned} e(r) &= \frac{v^2}{2} + \frac{5\mathcal{R}T}{2\mu} - \frac{GM_\star}{r} \\ &= e(r_0) + W(r) + q(r) \end{aligned} \tag{1.10}$$

which states that the total energy per unit mass, $e(r)$, is equal to the initial

energy, $e(r_0)$, at the lower boundary r_0, plus the energy added to the wind in the form of the work done by the force, $W(r)$, and the heat deposition, $q(r)$. In other words, the total energy added to the wind per unit mass is used to increase the kinetic energy and the enthalpy of the wind, and to lift it out of the gravitational potential well. We can also compare the energy of the wind at the photosphere and at infinity, as described by Lamers (1998). At the photosphere, the total energy is negative and is just the gravitational potential energy, because $v_{\rm esc} \gg \mathcal{R}T_\star/\mu$ and $v_{\rm esc} \gg v(R_\star)$, i.e.,

$$e(r_0) \simeq -\frac{GM_\star}{R_\star}. \tag{1.11}$$

At $r \to \infty$ the potential energy and the enthalpy both go to 0, and so the total energy is the kinetic energy,

$$e(r) \simeq \frac{{v_\infty}^2}{2}. \tag{1.12}$$

Substituting Equations 1.11 and 1.12 into Equation 1.10 then gives

$$\frac{{v_\infty}^2}{2} \simeq -\frac{GM_\star}{R_\star} + W(r) + q(r). \tag{1.13}$$

This equation tells us that a wind can only escape the gravitational potential of its star if there is an output force that provides sufficient momentum input or, if there is an energy source that provides sufficient heat input. These energy and momentum inputs are collectively known as wind driving mechanisms and in Section 1.4 we discuss the different mechanisms which occur across the H-R diagram.

1.4 Stellar Wind Driving Mechanisms Across the H-R Diagram

Stellar winds are a ubiquitous phenomenon across most of the H-R diagram. The various types of winds found throughout the H-R diagram can be broadly grouped into the three main categories of hot radiatively driven stellar winds, solar-type winds, and cool evolved stellar winds, as shown in Figure 1.3. The cool evolved

stellar winds can also be broadly grouped into the two categories of warm hybrid winds, and cool dense winds, as discussed in Section 1.2.

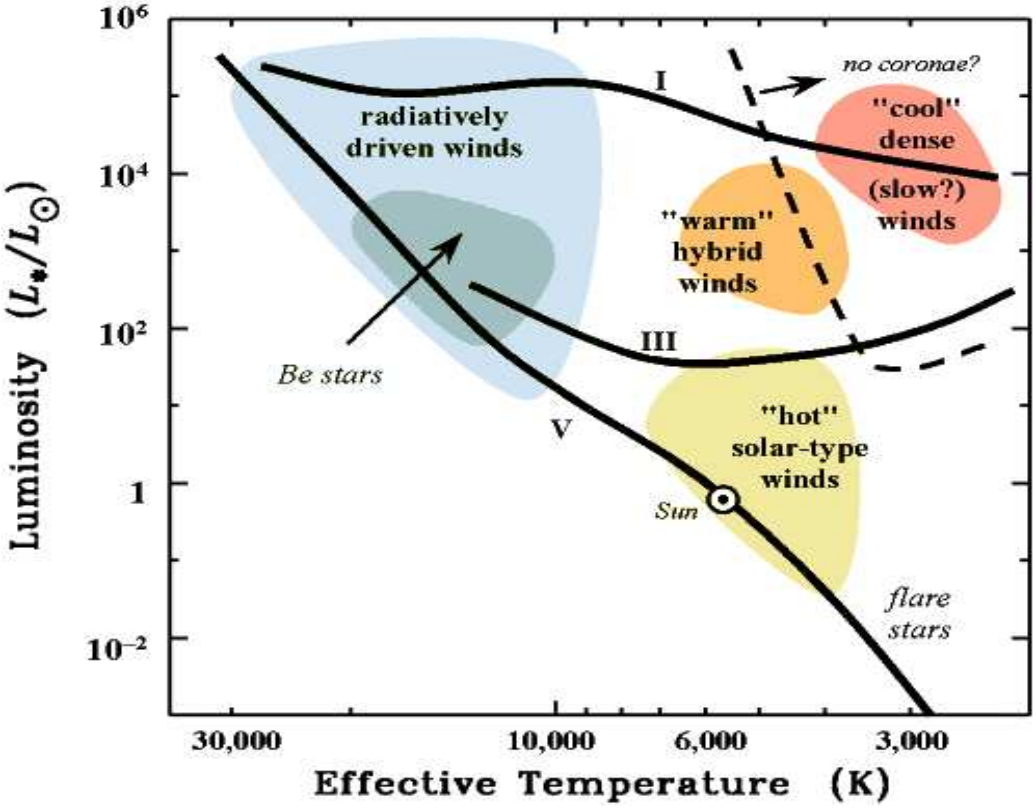

Figure 1.3: Stellar winds across the H-R diagram can be broadly grouped into the three main categories of hot radiatively driven stellar winds (upper left), solar-type winds (center right), and cool evolved stellar winds (upper right). The cool evolved stellar winds can also be broadly grouped into the two categories of warm hybrid winds (orange group) and non-coronal type (red group). *Image credit:* Steven Cranmer.

1.4.1 Radiatively Driven Winds

Stars earlier than spectral type ∼A2 emit their peak radiation in the UV, and so it was not until the early UV rocket observations that the presence of strong winds was confirmed from these stars (e.g., Morton, 1967). The broad P Cygni line profiles observed, indicated mass-loss rates as high as $10^{-5}\,M_\odot\,\mathrm{yr}^{-1}$ and wind terminal velocities up to $3500\,\mathrm{km\,s}^{-1}$. Even though the lifetime of these massive

hot stars is relatively short at just a few million years, their large mass-loss rates can substantially reduce the original stellar mass by a factor of two or more for the most massive (Owocki, 2004). Indeed, these stars typically end up as Wolf-Rayet (W-R) stars, which often appear to have completely lost their original envelope of hydrogen. These early-type stars do not exhibit the strong sub-surface convection that is present in solar and late-type stars (i.e., cool stars), and are therefore not believed to possess coronae. Their winds are therefore expected to remain at temperatures comparable to the star's surface, and so the gas-pressure term in Equation 1.4 is not sufficient to drive their winds. Instead these stars are known to have a high radiative flux (since this scales as the fourth power of the surface temperature), and Castor *et al.* (1975) showed that this flux can accelerate a time-steady wind, by coupling with optically think atomic lines in regions above the photosphere, where the continuum is optically thin. Therefore, the winds of these stars are effectively driven by the pressure of the star's emitted radiation and so the dominant term in Equation 1.4 is a radiation pressure term contained within the parameter f.

1.4.2 Solar Type Winds

Our understanding of the wind driving mechanisms for stars with *hot* solar-type winds is mainly based on solar theory and observations. Equation 1.4 was the cornerstone of many early attempts to explain the dynamics of the solar corona. Chapman & Zirin (1957) assumed a static corona (i.e., the acceleration term was zero) and that the pressure gradient was the only outward force (i.e., $f = 0$). Their results were unphysical, however, as they found that the density goes to infinity at large distances, and that the pressure was many orders of magnitude greater than that of the ISM. Parker (1958) assumed that there was a continuous isothermal outflow of material from the Sun caused only by the thermal pressure gradient term in Equation 1.4 (i.e., $f = 0$). He used the mass continuity equation, and the equation of state, to replace the pressure gradient term with a function depending only on velocity. Parker coined the solution to his simple analytical model as the "solar wind" and the predictions his model made for the solar velocity were confirmed shortly afterwards by some of the first space probes

(e.g., Neugebauer & Snyder, 1962). The assumptions of a radially expanding and isothermal outflow are not fully accurate in reality, however, and Parker's solution is an approximate characterization of the observed solar wind.

Coronal winds are generally tenuous, with mass-loss rates being too small to be of evolutionary importance. For example, at the Sun's current rate of mass-loss, about $10^{-14}\,M_{\odot}\,\mathrm{yr}^{-1}$, its mass would be reduced by only $\sim 0.01\%$ during its main sequence lifespan of $10^{10}\,\mathrm{yr}$. Wind velocities are generally high ($200 \rightarrow 800\,\mathrm{km\,s}^{-1}$), except for the very low gravity stars whose velocities are believed to be less Drake & Linsky (1986). Although Parker (1958) showed that the solar wind is a consequence of the thermal pressure gradient of the hot corona, the question of which mechanism drives the solar wind is still controversial, i.e., it is not understood how mechanical energy (convection) is transferred above the solar surface. The dissipation of Alfv́en waves is a reliable candidate as a primary source of coronal heating (Cranmer & Saar, 2011), although other sources of energy and momentum probably exist (e.g., Parker, 1983, 1988). These waves can transfer energy from the surface convection up to the wind acceleration region because they can travel longer distances due to their incompressible nature (e.g., Hollweg, 1973). The dissipation of these waves then transfer momentum and energy to the gas via a cascade from large to small eddies (Verdini & Velli, 2007). Evolved stars blueward of the Linsky-Haisch dividing line also posses coronae and may share a similar mass-loss mechanism to that of coronal stars on the main sequence.

1.4.3 Cool Evolved Stellar Winds

Cool evolved stars can generally be grouped into three main categories based on their mass and evolutionary status: (1) massive evolved red supergiants, (2) low and intermediate mass highly evolved stars ($0.8 - 8\,M_{\odot}$) known as asymptotic giant branch (AGB) stars, and (3) low and intermediate mass less evolved red giant stars. AGB stars lose a significant fraction of their mass through slow, massive winds at a rate of $10^{-8} \rightarrow 10^{-4}\,M_{\odot}\,\mathrm{yr}^{-1}$ (van Loon *et al.*, 2005). This mass-loss occurs as a result of stellar pulsations (Habing, 1996) which levitate

material from the stellar surface, followed by the acceleration of dust grains by radiation pressure (Gehrz & Woolf, 1971).

The mass-loss mechanisms operating in red giants and red supergiants remain largely unknown and the theory governing mass-loss in AGB stars is not appropriate (Josselin & Plez, 2007). Red giants and red supergiants have small amplitude variations and so they do not pulsate in a similar manner to AGB stars. Also, significant amounts of dust are only found at large radii for red supergiants (Danchi *et al.*, 1994), while red giants may have little or no dust in their outflows (Jones, 2008). One of the most plausible mass-loss mechanisms for these stars over the past few decades has been the transfer of energy and momentum to the wind by the dissipation of Alfvén waves. Unlike acoustic waves, Alfvén waves have large damping lengths that can transfer energy and momentum to the gas over many stellar radii. Alfvén wave models were original known to result in high velocity winds, unlike what is observed for cool evolved stars. Hartmann & MacGregor (1980) successfully showed that these observed low outflow velocities and high mass-loss rates could be reproduced if a wave damping mechanism is effective close ($r < 2\,R_\star$) to the star. Hartmann & Avrett (1984) constructed an Alfvén wave model for the red supergiant Betelgeuse which predicted its wind to have an electron temperature of 8000 K at $4\,R_\star$ and remaining above 5000 K out to $10\,R_\star$. However, the radio observations of Lim *et al.* (1998) revealed a much cooler wind cooler wind (see Chapter **??**) in conflict with the models of Hartmann & Avrett (1984). Also, the semi-empirical model of Harper *et al.* (2001) found the wind to be only lightly ionized, which means that Alfvén waves, which couple only to ionized gas, are unlikely to be capable of transferring the required energy and momentum to the winds of red supergiants; although they still may be important for the less massive red giants. One current school of thought is that giant convection cells may initiate the mass-loss process in red supergiants (e.g., Lim *et al.*, 1998), although currently no model exits to explain how such a mechanism could operate.

1.5 Red Giant and Red Supergiant Evolution

Once a star has exhausted the hydrogen in its core, it evolves off the main sequence and spends the majority of its post-main sequence lifetime either as a red giant or a red supergiant (RSG). The vast majority of stars are of either low to intermediate mass (i.e., $M_\star \lesssim 8\,M_\odot$), and evolve to become red giants, while the rare massive stars (i.e., $M_\star \gtrsim 8\,M_\odot$) generally evolve to become red supergiants. These evolved late-type stars contain a condensed core with an extended envelope and have cooler effective temperatures than when on the main sequence. There is currently no consensus in the scientific community on why stars become red giants or red supergiants (e.g., Stancliffe *et al.*, 2009; Sugimoto & Fujimoto, 2000). A common explanation is that the initial expansion is driven by the envelope maintaining thermal equilibrium in response to increasing luminosity from the core. This expansion causes local cooling, allowing heavy elements to recombine, therefore causing an increase in opacity. This increase in opacity traps energy leading to a runaway expansion that brings the star to the red giant or red supergiant region of the H-R diagram (Renzini *et al.*, 1992). However, Iben (1993) computed evolutionary models for intermediate mass stars with with the opacity held constant throughout, and showed that these models still became giants. This meant that opacity was not responsible for transition to a red giant, apparently in contradiction to Renzini *et al.* (1992).

1.5.1 Change in Atmospheric Dynamics

The expansion of a star's radius as it evolves off the main sequence greatly affects the dynamics of its atmosphere through the change of surface gravity. The decrease in surface gravity causes the density scale height to increase, resulting in very extended atmospheres. The mass-loss rate also increases due to the increase in the stellar surface area ($\propto R_\star^2$) and the increase of the density. In Table 1.1 we describe the typical properties of a 1 and 15 $M_\odot$ star both on the main sequence and as an evolved late-type star. We use these as examples to highlight the changes in the atmospheric dynamics when a star becomes a red giant or red supergiant. For these stars, the massive increase in stellar radius means that the density scale height, H_ρ, as a fraction of the stellar radius, $H_\rho/R_\star \propto T_{\rm eff} R_\star$, is

~ 2 orders of magnitude greater than when on the main sequence. There is also a drastic change in the terminal wind velocity, v_∞. While on the main sequence, hot massive stars have wind velocities that are many times the photospheric escape velocity, $v_{\rm esc}$, while solar type stars have terminal wind speeds close to $v_{\rm esc}$. For evolved late-type stars the terminal wind velocity is generally much less than the photospheric escape velocity, signaling that the onset of these winds must be at several stellar radii. The final column in Table 1.1 is a comparison of the integrated mass-loss of these stars while on and off the main sequence. It is clear that during the time, t, spent in these evolved states, these stars lose a significant proportion of their initial mass, i.e., $\sim 30\%$ for massive stars and $\sim 10\%$ for the lower to intermediate mass stars. Such large quantities of mass-loss must have a significant impact on the evolution of the stars themselves and on their surrounding environments.

Table 1.1: Typical properties for main sequence and evolved 15 and 1 $M_\odot$ stars.

Evolutionary Stage[a]	$R_\star$ ($R_\odot$)	$H_\rho/R_\star$	v_∞ (km s^{-1})	$v_{\rm esc}$ (km s^{-1})	t (yr)[b]	$\dot{M}_\star$ ($M_\odot$ yr^{-1})	$t \times \dot{M}_\star$ ($M_\odot$)
MS O/B	5	10^{-4}	3000	1000	10^6	10^{-6}	1
RSG	1000	10^{-2}	20	75	5×10^5	10^{-5}	5
MS F/G	1	10^{-4}	400	600	10^{10}	10^{-14}	10^{-4}
RG	40	10^{-2}	40	100	10^9	10^{-10}	0.1

[a] MS O/B = main sequence spectral type O and B stars. RSG = red supergiant. MS F/G= main sequence spectral type F and G stars. RG = red giant.

[b] The lifetimes for the evolutionary phases of the massive star are taken from Stothers & Chin (1969)

1.5.2 Evolutionary Tracks

Once a massive star on the main sequence has exhausted its hydrogen core, it follows a nearly horizontal evolution across the H-R diagram where it usually becomes a helium burning RSG. Examples of these horizontal evolutionary tracks are shown in Figure 1.4 for masses between 9 and 120 $M_\odot$. Once the massive blue hydrogen burning stars move off the main sequence, they rapidly evolve across the "yellow void" passing through the very short-lived yellow supergiant stage

(Levesque, 2010). As these stars evolve, the luminosity remains almost constant because massive stars do not develop degenerate cores and most of the mass is in radiative equilibrium. For stars with main sequence masses $\lesssim 25\,M_{\odot}$, like Betelgeuse, the RSG phase is the final stage before ending their lives as hydrogen-rich Type II supernovae. These stars loss a few $M_{\odot}$ during the RSG phase but do not lose enough to remove the whole H-rich envelope. Stars with masses $25\,M_{\odot} \lesssim M_{\star} \lesssim 40\,M_{\odot}$ loose their H-rich envelope during the RSG stage, turning the star into a W-R star. Finally, stars with $M_{\star} \gtrsim 40\,M_{\odot}$ never becomes RSGs as their H-rich envelopes are blown off before the RSG stage can be reached.

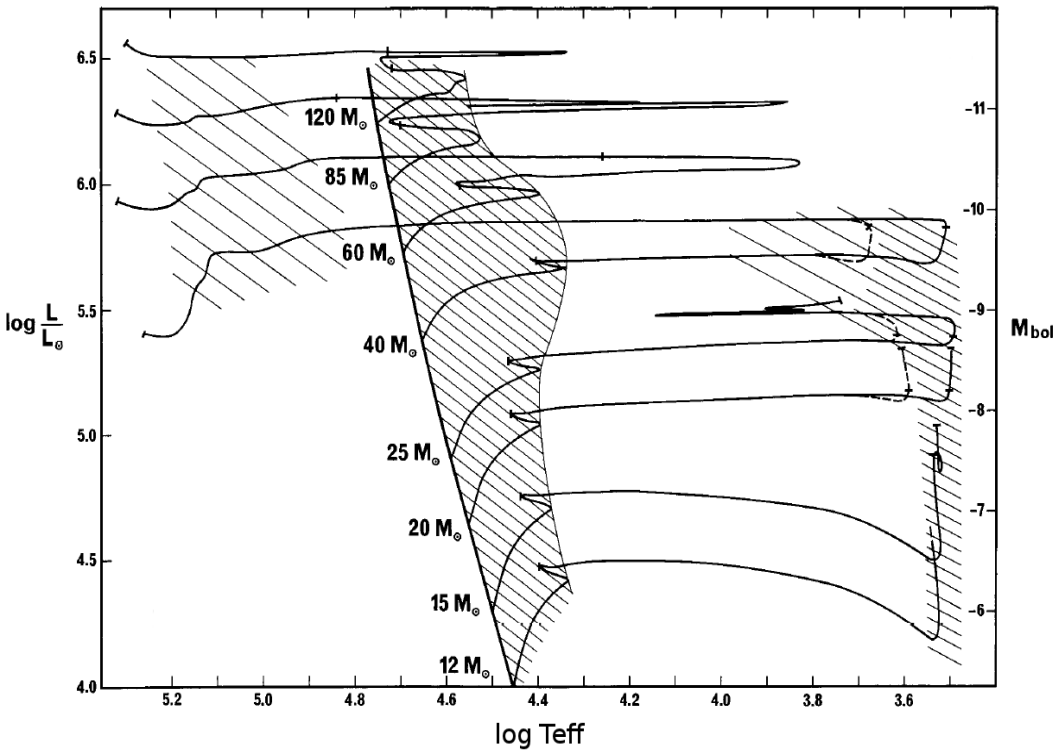

Figure 1.4: Evolutionary tracks of massive stars from Maeder & Meynet (1987). The shaded regions correspond to long-lived evolution phases on the main sequence, and during core He burning as a RSG (at $\log T_{\rm eff} < 4.0$) or as a W-R star (at $\log T_{\rm eff} > 4.8$).

For stars with $M_{\star} \lesssim 8\,M_{\odot}$, like Arcturus and Aldebaran, the post main sequence evolution can generally be categorized into four main stages as shown in

Figure 1.5.

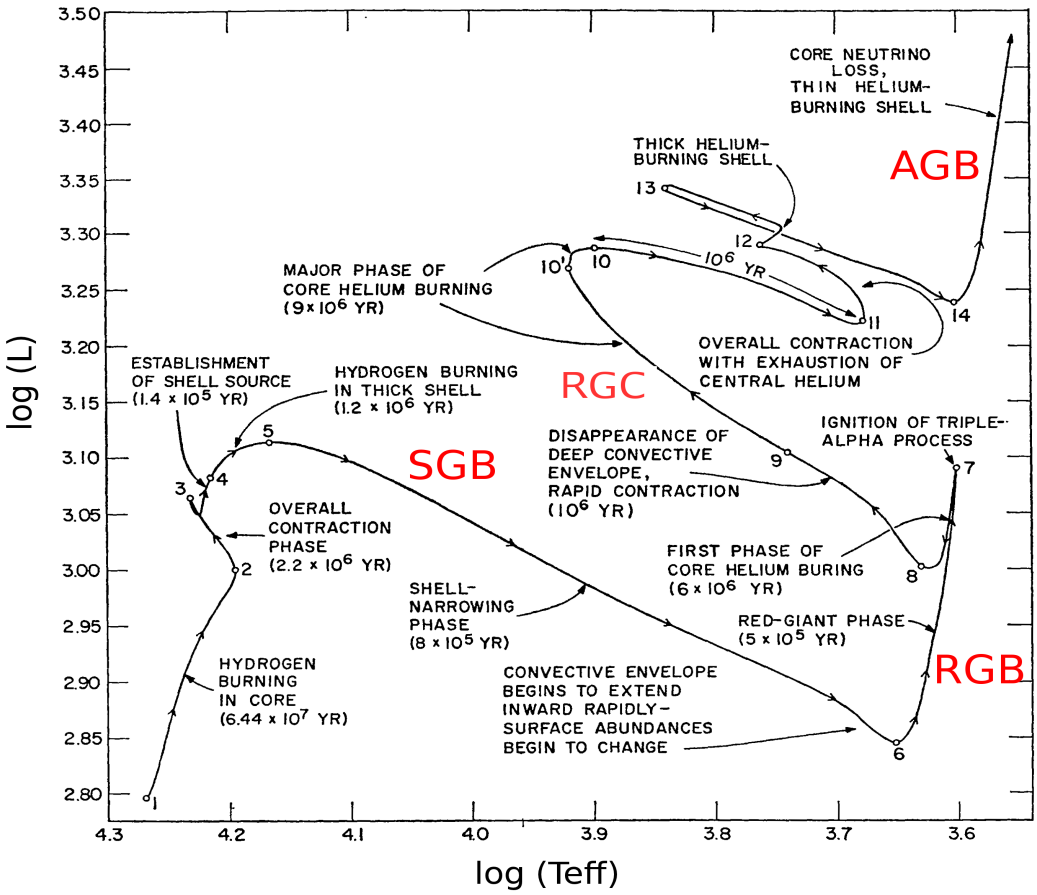

Figure 1.5: Evolutionary track for $5\,M_\star$ star. Luminosity is in solar units and temperature is measure in Kelvin. For stars with $M_\star \lesssim 8\,M_\odot$, the post main sequence evolution can generally be categorized into four main stages, i.e., the subgiant branch (SGB), the red giant branch (RGB), the red giant clump (RGC), and the asymptotic giant branch (AGB). The time spent at each stage of evolution depends on the main sequence mass. Figure is from Iben (1967).

1. The Subgiant Branch (SGB) - Points $2 \rightarrow 6$: This stage defines the period when a star has stopped core hydrogen burning but has not yet begun core helium burning. The core contracts therefore increasing the star's central temperature enough to initiate hydrogen fusion in a shell surrounding the core. The star swells and the effective temperature drops as it moves rapidly across the SGB resulting in the Hertzsprung Gap.

2. The Redgiant Branch (RGB) - Points 6 $\rightarrow$ 8: As a star moves up the RGB its luminosity increases dramatically. The H-burning shell experiences a large gravitational force from the dense contracting core, causing the shell to compress and increase its energy output. A deep convective outer envelope penetrates the inner layers containing the remnants of H-burning resulting in newly synthesized nuclei being transported to the surface. This process is called the "first dredge-up". At the tip of the RGB, the core finally reaches a high enough temperature to cause helium burning, igniting the triple alpha process. The core begins to expand and the outer layers of the star contract, raising the surface temperature and leading to the output of less shell energy. This leads to a momentary decrease in luminosity (points 7 to 8) and the star moves off the RGB.

3. The Redgiant Clump (RGC) - Points 8 $\rightarrow$ 14: Core helium burning and hydrogen shell burning characterize the RGC. A stars position on the RGC depends on its initial mass and composition, and also on the amount of mass it has lost during the red giant phase. The pressure increases on the H-burning shell from the contracting envelope above, leading to an overall increase in luminosity. Core He-burning leads to an increasing molecular weight of the gas in the core, causing it to eventually contract (point 10'). At the end of the RGC phase, all of the helium in the core is exhausted. The core collapses and the temperature rise ignites a shell of He-burning. The expanding star cools enough for convection to again penetrate the inner layers, causing the "second dredge-up". The cooling, convective star now approaches the asymptotic giant branch.

4. The Asymptotic Giant Branch (AGB) - Points 14 $\rightarrow$ ... : The AGB is marked by a C-O core with two burning shells of He and H. The C-O core continues to grow and contract as the adjacent He shell burns. With both shells burning, energy is consumed at an ever increasing pace and the star rapidly moves up the AGB while also developing periodic instabilities and generating large mass-loss rates. Stars of masses greater than about $2\,M_{\odot}$ will end up with their surface convection zone connecting with the convecting core, causing a "third dredge-up". For stars with masses less

than about $8\,M_{\odot}$, their cores never reach high enough temperatures to burn C-O and their evolution stops on the AGB. Higher mass stars can continue the process until iron is generated in the core and the evolution has gone as far as it can go.

Traditionally, it has been almost impossible to distinguish between red giants burning helium in the core and those burning only hydrogen in an outer shell. Asteroseismology, is now becomming a powerful tool to help probe the internal structures of stars using their natural oscillation frequencies (Beck *et al.*, 2011) and has recently been used to distinguish between hydrogen and helium buring red giants (Bedding *et al.*, 2011). In this thesis, the term red giant refers to evolved stars with $M_{\star} \lesssim 8\,M_{\odot}$ which have not reached the AGB stage of evolution.

1.6 Radio Emission from Stellar Atmospheres

If we assume the Sun to be a nearly ideal blackbody with temperature $T = 5800\,K$, then at 10 GHz (i.e., 3 cm), its flux density at Earth would be $\sim 10^6$ Jy. However, at the distance of the nearest star other than the Sun (i.e., ~ 1.3 pc), its flux density would be only $\sim 15\,\mu$Jy. Such a value would have been impossible to detect with even the most powerful radio telescopes up until recently[1]. Nevertheless, stars have been detected at radio wavelengths for decades which tells us immediately that such stars behave differently to the Sun at radio wavelengths. In fact, the discovery that such a huge range of stars emit detectable radio emission was one of the major and unexpected achievements of the old VLA (White, 2000). A sample of the radio detected stars is plotted on a H-R diagram in Figure 1.6 with the filled symbols representing the non-thermal emitters, and the open symbols representing the thermal emitters.

It is clear that the majority of the main sequence and subgaint objects are non-thermal emitters. The only thermal emitters on the main sequence are the massive hot O-B stars which emit free-free radiation from their dense and ionized winds (e.g., Scuderi *et al.*, 1998). Their radio spectrum are generally in good agreement with constant velocity isothermal stellar winds (i.e., $F_{\nu} \propto \nu^{0.6}$

[1]The new VLA has the ability to detect such values

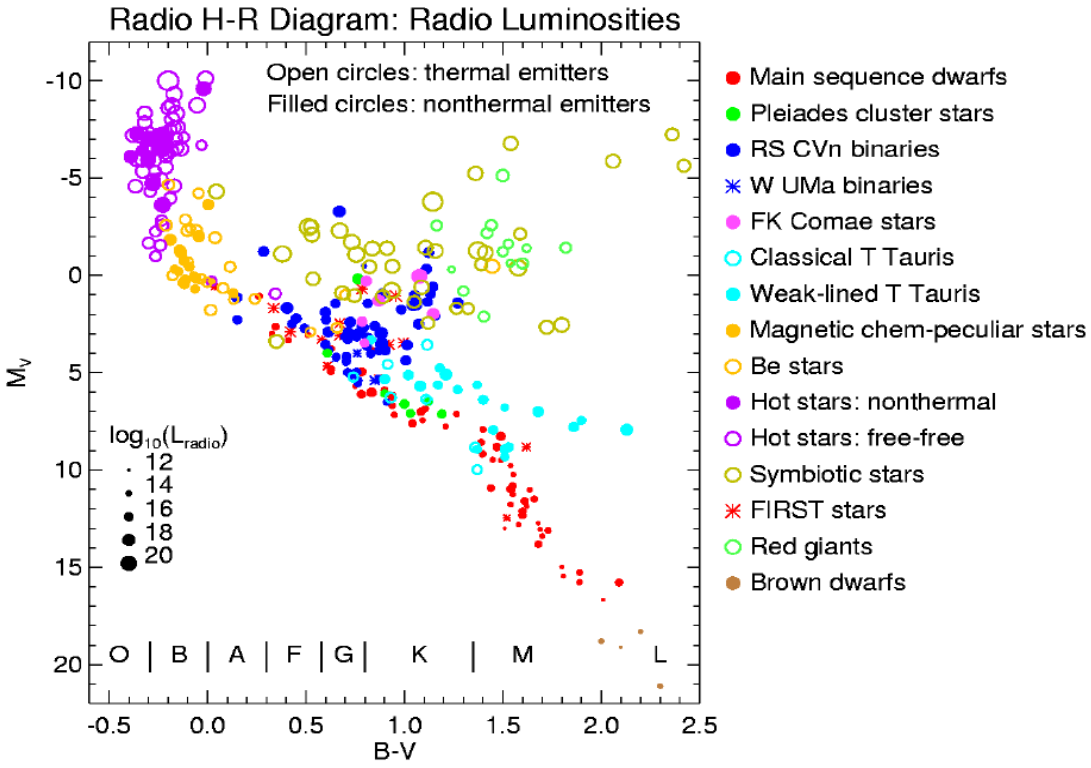

Figure 1.6: Sample of the radio detected stars plotted on a H-R diagram. The filled symbols represent non-thermal emitters while the open symbols represent the thermal emitters. The larger symbols are more radio luminous than the smaller symbols. In general, the sparse thermal emitters are stars with ionized or partially ionized extended stellar atmospheres whose radio emission comes from free-free interactions. Figure from White (2000).

as discussed in Section 1.8.4). These massive hot stars also emit non-thermal emission which is believed to be produced by electron shock acceleration in the inhomogeneous wind. The cool region of the main sequence in Figure 1.6 contains red filled dots representing young F, G, K, and M dwarfs. These objects have "non-thermal coronae", which in addition to thermal populations of electrons at 10^{6-7} K, contain non-thermal populations, which are trapped on closed magnetic field lines and produce strong radio emission. These objects are also flare stars, meaning that they occasionally emit strong radio outbursts. The blue filled circles near the center of the diagram are RS CVn binaries which consist of a late-type

giant or subgiant and a close binary companion (Strassmeier *et al.*, 1993). These systems generally rotate fast with typical orbital periods of a few days. Tidal forces between the close components have locked their rotational periods to the orbital period. This fast rotational period in combination with outer convective zones generate intense magnetic activity and radio emission.

Single (non-binary) cool evolved stars lack the characteristics which make the other stars, described above, radio bright. Even though they have convective zones, they rotate too slowly to generate, via a dynamo, the magnetic activity which make subgiant binaries and young cool dwarfs strong non-thermal radio emitters. They also lack the intense UV radiation field of the massive hot main sequence stars and their outflows are generally only weakly ionized. However, their large angular diameters coupled with their relatively large mass-loss rates, means that their partially ionized outflows can be detected at radio wavelengths. Red giants are feeble radio emitters however and up until this thesis, only a small number have been detected at one or more radio wavelengths, and these have been modest S/N measurements. On the other hand, a few close-by red supergiants, like Betelgeuse, have mass-loss rates many orders of magnitude greater than the red giants and their partially ionized outflows can be easily detected at multiple radio wavelengths. These red supergiants also contain extended circumstellar envelopes (CSEs) which can be sources of molecular line emission at radio wavelengths. Prior to this thesis, these CSEs have only been studied with single dish radio antennas providing little or no spatial information on the gas distribution.

1.7 Radio Emission Mechanisms

The two radio emission mechanisms which are of most relevance in this thesis are thermal Bremsstrahlung/free-free emission, and molecular line emission. Both of these emission mechanisms produce incoherent radiation and are discussed in the following sections. Under certain plasma conditions, coherent radiation can be produced due to resonances between particles and characteristic waves. This results in electron energy being converted into some natural wave mode of the

plasma, such as Langmuir waves (plasma oscillation) or electron-cyclotron waves. The main characteristic frequencies of a plasma are the electron plasma frequency

$$\nu_p = \frac{\omega_p}{2\pi} = \left(\frac{n_e e^2}{\pi m_e}\right)^{1/2} \approx 9000 n_e^{1/2} \quad \text{Hz} \tag{1.14}$$

and the electron-cyclotron frequency

$$\nu_B = \frac{\Omega_B}{2\pi} = \frac{eB}{2\pi m_e c} \approx 2.8 \times 10^6 B \quad \text{Hz} \tag{1.15}$$

where n_e is the electron number density with units cm^{-3}, and B is the magnetic field strength with units G.

1.7.1 Thermal Free-free (Bremsstrahlung) Emission

Thermal Bremsstrahlung from an ionized or partially ionized plasma is often called free-free emission because it is produced by free electrons which are deflected off ions without being captured. For free-free radio emission, the distant Coulomb interactions of electrons with ions, which cause small angle deflections, are much more important than the rare close encounters and large deflections (Dulk, 1985). The free-free emission, which is the energy radiated per unit volume, per unit time, per unit frequency, is given in Rybicki & Lightman (1979) as:

$$\varepsilon_\nu^{ff} = 6.8 \times 10^{-38} Z^2 n_e n_i T^{-1/2} e^{-h\nu/kT} g_{ff} \quad \text{erg cm}^{-3}\,\text{s}^{-1}\,\text{Hz}^{-1} \tag{1.16}$$

Here, g_{ff} is the free-free Gaunt factor and is a correction factor which is a function of electron energy and frequency of emission. Extensive tables and graphs of g_{ff} exist in the literature (e.g., Karzas & Latter, 1961). The free-free emissivity, which is a fundamental term in the equation of radiative transfer is then

$$j_\nu^{ff} = \frac{\varepsilon_\nu^{ff}}{4\pi}. \tag{1.17}$$

The free-free radio opacity can be found from Kirchoff's law and is discussed in Section 1.8.3.

1.7.2 Molecular Line Emission

A diatomic molecule such as CO or SiO, can vibrate (stretch) along the internuclear axis and can also undergo rotational motion around an axis perpendicular to the internuclear axis. The rotational levels of these molecules are designated by a single vibrational quantum number, v, and rotational quantum number, J. Most of the diatomic molecular lines observed in the radio spectrum are from the rotational levels. These rotational energy levels are approximately those allowed by quantum mechanics for a rigid rotator, i.e., a linear molecule that does not change shape as it rotates. The rotational kinetic energy is

$$E_{\rm rot} = \frac{I\omega^2}{2} \tag{1.18}$$

where $I = m_r r_0^2$ is the moment of inertia, m_r is the reduced mass, r_0 is the separation of the two masses, and ω is the angular velocity of the rotation. The quantization of angular momentum, L, to integer multiples of $\hbar$ leads to $L = J\hbar$, where $J = 1, 2, \ldots$. Equation 1.19 can then be written as

$$E_{\rm rot} = \frac{L^2}{2I} = \frac{J(J+1)\hbar^2}{2I} = \frac{J(J+1)\hbar^2}{2m_r r_0^2} = B_v J(J+1) \tag{1.19}$$

where B_v is the *rotation constant* and is subscripted v because the moment of inertia depends on the vibrational state.

Pure rotational transitions, $J \rightarrow J-1$, have energy $h\nu = 2B_v J$. It is straightforward to show that the rotational transitions $J = 1-0$ and $J = 2-1$ of the CO molecule results in spectral lines at frequency 115.2712 and 230.5424 GHz. A radio spectrum of a particular molecular species will resemble a *ladder* as shown in Figure 1.7. Each step in the plot are all harmonics of the fundamental frequency that is determined solely by the moment of inertia of that species. As $\nu \propto m^{-1} r_0^{-2}$, large heavy molecules in CSEs may be seen at centimeter wavelengths, but smaller and lighter molecules such as CO and SiO emit only at millimeter wavelengths. If the critical density is low (i.e., $C_{j,j-1} > A_{j,j-1}$), where

$$A_{j,j-1} = 1.07 \times 10^{-7} \frac{J^4}{J+1/2} \quad {\rm s}^{-1} \tag{1.20}$$

(Draine, 2011), then the rotational levels are in thermal equilibrium and the Boltzmann equation can be used to find the relative populations of the levels. The partition function, $Z(T)$, is found by summing over all levels, i,

$$Z(T) = \sum_i g_i e^{-E_i/kT} \tag{1.21}$$

$$= \sum_{J=0}^{J=i} (2J+1) e^{-BJ(J+1)/kT} \tag{1.22}$$

$$\approx \int_0^\infty (2J+1) e^{-BJ(J+1)/kT} dJ = kT/B. \tag{1.23}$$

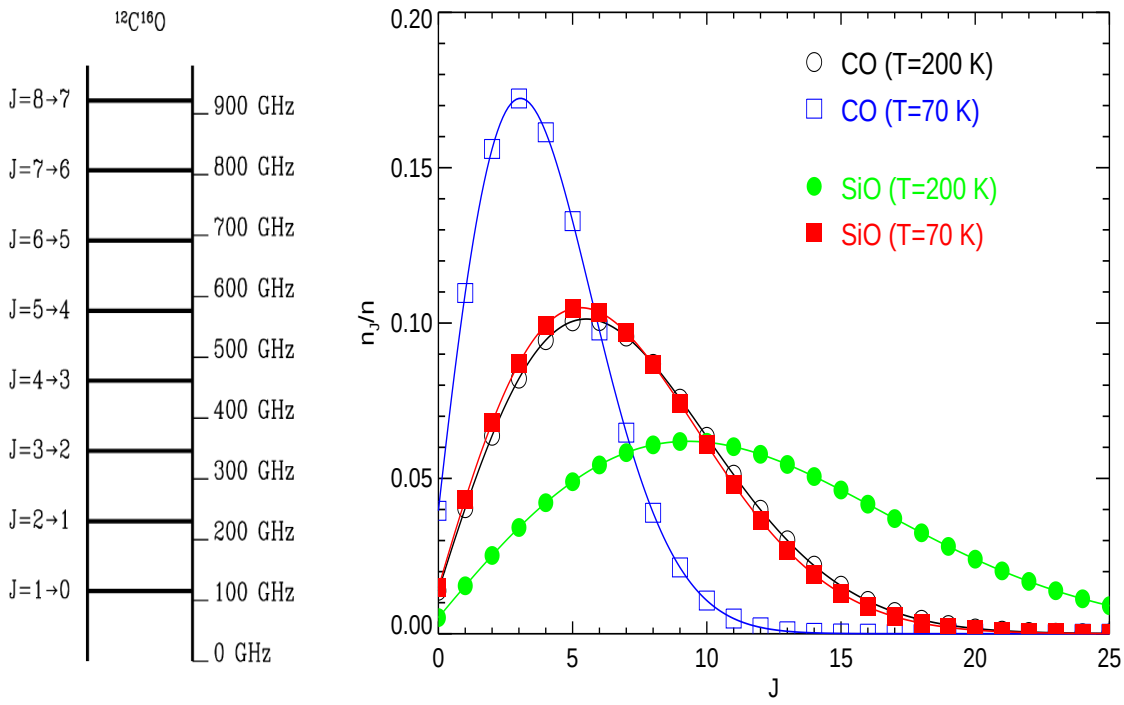

Figure 1.7: *Left:* The radio spectrum of $^{12}C^{16}O$ resembles a *ladder* with each step being a harmonic of the fundamental frequency that is determined solely by the moment of inertia. This molecule has a relatively small moment of inertia and therefore has no cm-wavelength lines. *Right:* The relative populations of the rotational levels of CO and SiO at temperatures of 70 and 200 K. At lower temperatures, the distribution of the relative populations of the rotational levels is towards lower Js and is shifted towards higher Js at higher temperatures.

The relative rotational populations within a given vibrational state are then

$$\frac{n_J(v)}{n(v)} \approx \frac{(2J+1)B}{kT} e^{-BJ(J+1)/kT} \tag{1.24}$$

which depends only on T. This distribution is plotted in Figure 1.7 for the ground vibrational levels of CO and SiO and shows how the levels are populated with respect to one another at two different temperatures[1]. The distribution is such that at low temperatures, the rotational levels are more relatively populated at lower Js, while higher Js become relatively more populated at higher temperatures.

1.8 Radio Observations of Stellar Atmospheres

In the following sections we present the basic definitions used to describe radio observations of stellar atmospheres. We define the *brightness temperature* which is commonly used in radio astronomy to measure the brightness of a source, along with its relationship to the fundamental quantity measured by a radio telescope, the *flux density*. Focusing on thermal emission, we describe how the flux density varies with frequency when observing both optically thin and optically thick stellar atmospheres.

1.8.1 Brightness Temperature

In thermodynamic equilibrium the spectral distribution or brightness, B_ν, of the radiation of a black body with temperature T_e is given by the Planck law

$$B_\nu(T_e) = \frac{2h\nu^3}{c^2} \frac{1}{e^{h\nu/kT_e} - 1} \tag{1.25}$$

and has units of flux per frequency interval per solid angle. One can easily switch to a wavelength scale using $B_\nu d\nu = B_\lambda d\lambda$. When $h\nu \ll kT_e$ Equation 1.25 becomes the *Rayleigh-Jeans Law*

$$B_\nu(T_e) = I_\nu(T_e) = \frac{2\nu^2 kT_e}{c^2}. \tag{1.26}$$

[1] These temperatures are the expected values of the CSE flows of Betelgeuse.

This equation does not contain Plank's constant and therefore is the classical limit of the Planck Law. We have also included the specific intensity, I_ν, here as it has the same units as the spectral brightness and for blackbody radiation, $I_\nu(T_e) = B_\nu(T_e)$. This equation is valid for all thermal radio sources except in the millimeter or sub-millimeter regime at low temperatures (Rohlfs & Wilson, 1996). In the Rayleigh-Jeans relation, the brightness is strictly proportional to the thermodynamic temperature of the black body. In radio astronomy it is customary to measure the brightness of an object by its *brightness temperature*, T_b. Therefore, the brightness temperature is the temperature at which a blackbody would have to be in order to reproduce the observed brightness of an object at frequency ν and is defined as

$$T_\mathrm{b} = \frac{c^2}{2k\nu^2} I_\nu. \tag{1.27}$$

If $h\nu/kT \ll 1$ and if I_ν is emitted by a blackbody, then T_b is the thermodynamic temperature of the source. If other processes are responsible for the emission or if the frequency is so high that Equation 1.26 is not valid, then T_b is different from the thermodynamic temperature of a black body.

The equation of radiative transfer describes the change in specific intensity of a ray along the line of sight in a slab of material of thickness ds

$$\frac{dI_\nu}{ds} = j_\nu - \kappa_\nu I_\nu, \tag{1.28}$$

where j_ν and κ_ν are the emissivity (in $\mathrm{erg\,s^{-1}\,cm^{-3}\,Hz^{-1}\,sr^{-1}}$) and the absorption/opacity coefficient (in $\mathrm{cm^{-1}}$) of the plasma. In thermodynamic equilibrium the radiation is in complete equilibrium with its surroundings and the brightness distribution is described by the Planck function

$$\frac{dI_\nu}{ds} = 0, \qquad I_\nu = \frac{j_\nu}{\kappa_\nu} = B_\nu(T_e). \tag{1.29}$$

Equation 1.28 can be solved by first defining the optical depth, $d\tau_\nu$, as

$$d\tau_\nu = -\kappa_\nu ds, \tag{1.30}$$

and then integrated by parts between 0 to s, and τ to 0, to give

$$I(s) = I(0)e^{-\tau(s)} + \int_{\tau(s)}^{0} e^{-\tau}\frac{j_\nu}{\kappa_\nu}d\tau. \tag{1.31}$$

The second term within the integral is known as the source function, S_ν, and this can be taken outside of the integral in the case of a homogeneous source, i.e., one for which both the emissivity and absorption coefficient are constant along the ray path. The solution then to the equation of radiative transfer for a homogeneous source is

$$I_\nu = I_0 e^{-\tau} + \frac{j_\nu}{\kappa_\nu}(1 - e^{-\tau}). \tag{1.32}$$

Using Equations 1.27 and 1.29 one obtains

$$T_b = T_0 e^{-\tau} + T_e(1 - e^{-\tau}). \tag{1.33}$$

This equation assumes thermodynamic equilibrium and so only holds for a thermal source. If T_e is replaced with $T_{\rm eff} = h\nu/k$ then this equation becomes valid for a homogeneous nonthermal source, i.e.,

$$T_b = T_0 e^{-\tau} + T_{\rm eff}(1 - e^{-\tau}). \tag{1.34}$$

For an isolated thermal source, there are two limiting cases:

$$T_b = T_e \quad \text{(i.e., for optically thick } \tau \gg 1) \tag{1.35}$$

and

$$T_b = \tau T_e \quad \text{(i.e., for optically thin } \tau \ll 1). \tag{1.36}$$

In these equations, T_e can also be replaced by $T_{\rm eff}$ if the radio emission emission is non-thermal. Also, these equations are only valid if the source is spatially resolved. If the source is unresolved then an upper limit to $T_e/T_{\rm eff}$ is found.

1.8.2 Brightness Temperature and Flux Density

The flux density, F_ν, is a fundamental quantity measured by a radio telescope and is usually measured in Janskys (Jy) where $1\,\mathrm{Jy} = 1 \times 10^{-26}\,\mathrm{W\,m^{-2}\,Hz^{-1}}$. The

observed flux density measured by the radio telescope is

$$F_\nu = \int_\Omega I_\nu \, d\Omega \tag{1.37}$$

where Ω is the solid angle subtended by the star. The radio emission from evolved cool stars is almost purely thermal and so Equation 1.37 becomes

$$F_\nu = \frac{\pi R_\star^2}{d^2} \frac{2k\nu^2 T_b}{c^2}. \tag{1.38}$$

The angular diameter of a star in radians is $\phi_\star = 2R_\star/d$ and so

$$F_\nu = \frac{\pi k \phi_\star^2 T_b}{2\lambda^2} \tag{1.39}$$

If $\phi_\star$ has major and minor axes $\phi_{\rm maj}$ and $\phi_{\rm min}$ then

$$T_b(K) = 1.96 F_\nu({\rm mJy}) \left(\frac{\lambda}{\rm cm}\right)^2 \left(\frac{\phi_{\rm min}}{\rm arcsec} \frac{\phi_{\rm min}}{\rm arcsec}\right)^{-1}. \tag{1.40}$$

Therefore, if an optically thick stellar atmosphere can be spatially resolved (i.e., $\phi_{\rm maj}$ and $\phi_{\rm min}$ can be measured) then the flux density at a particular wavelength tells gives the brightness temperature and therefore the electron temperature. Unfortunately, the number of stars that can have their atmospheres spatially resolved at radio wavelengths is low due to their relatively small angular diameters. However, different layers of stellar atmospheres can still be probed due to the nature of the free-free radio opacity which is discussed in the next section.

1.8.3 Thermal Free-free Radio Opacity

In Section 1.7.1 we gave an expression for the thermal free-free emissivity of an ionized gas. Since we assumed LTE at some temperature T, we can use Kirchoff's law to find the thermal radio free-free opacity (absorption coefficient):

$$\frac{j_\nu^{ff}}{\kappa_\nu^{ff}} = \frac{2h\nu^3}{c^2} \frac{1}{e^{h\nu/kT} - 1} \tag{1.41}$$

Using Equation 1.16 and 1.19 then provides a value for the free-free radio opacity

$$\kappa_\nu^{ff} = \frac{0.018 Z^2 n_e n_i g_{ff}(\nu, T_e)}{T_e^{1.5}\nu^2} \quad \text{cm}^{-1}. \tag{1.42}$$

The Gaunt factor is slightly dependent on temperature and frequency and at cm-wavelengths is given by

$$g_{ff}^{cm} = 11.96 T_e^{0.15}\nu^{-0.1} \tag{1.43}$$

(Altenhoff *et al.*, 1960), while in the sub-millimeter regime it is slightly different

$$g_{ff}^{sub-mm} = 24.10 T_e^{0.26}\nu^{-0.17} \tag{1.44}$$

(Hummer, 1988). The abundant species in the atmospheres of cool evolved stars are either neutral or single ionized so that $Z = 1$ and $n_e = n_i$. Focusing on centimeter wavelengths, the radio opacity is then

$$\kappa_\nu^{ff} = \frac{0.212 n_e^2}{T_e^{1.35}\nu^{2.1}} \quad \text{cm}^{-1}. \tag{1.45}$$

Therefore, the free-free opacity increases towards lower frequencies as $\kappa_\nu^{ff} \propto \nu^{-2.1}$ (or longer wavelengths as $\kappa_\lambda^{ff} \propto \lambda^{2.1}$). This means that the optical depth, $\tau_\lambda = \int \kappa_\lambda dr$, also increases towards longer wavelengths implying that the effective radius (i.e., the radius where $\tau_\lambda = \tau_{\text{radial}}$) will increase with longer wavelengths. As a result, different layers of unresolved stellar atmospheres can be probed by observing them at different radio wavelengths.

In LTE, the solution to the equation of radiative transfer (i.e, Equation 1.32) for a plasma with no background source can be written as

$$I_\nu = B_\nu(1 - e^{-\tau}). \tag{1.46}$$

An example of such a source is an isolated H II region. At long enough wavelengths the H II region becomes opaque so that $\tau_\nu \gg 1$. Equation 1.46 then tells us that the spectrum approaches that of a black body with a flux density varying as $F_\nu \propto \nu^2$. At short wavelengths where $\tau_\nu \ll 1$, the H II region is almost

transparent, and the flux density becomes

$$F_\nu \propto \frac{2kT_e\nu^2}{c^2}\tau_\nu \propto \nu^{-0.1}. \tag{1.47}$$

These two scenarios are shown in Figure 1.9 along with the point where these two slopes intersect which corresponds to the frequency at which $\tau \simeq 1$. When the radio spectrum is plotted on a log-log plot as in Figure 1.8, the spectral slope is referred to as the spectral index, α, and is defined:

$$\alpha = \frac{d\log F_\nu}{d\log \nu}. \tag{1.48}$$

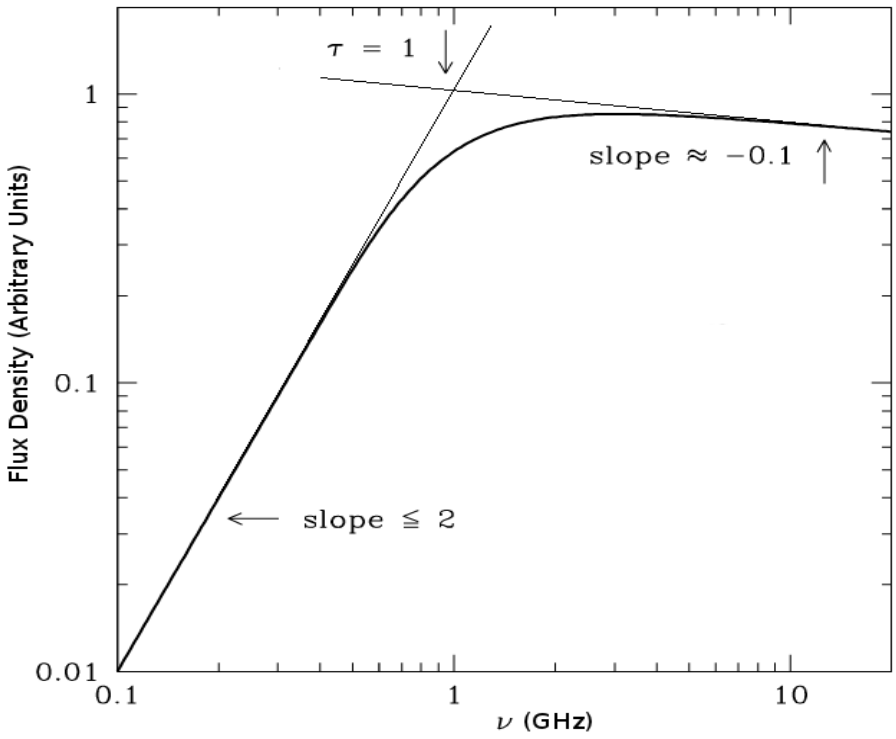

Figure 1.8: The radio spectrum for a hypothetical H II region with no background illuminating source. At long wavelengths the source becomes opaque and has a black body like spectrum with $\alpha = 2$. At short wavelengths where $\tau_\nu \ll 1$, the H II region is almost transparent and $\alpha = -0.1$. Image adapted from NRAO's *Essential Radio Astronomy* course.

1.8.4 Radio Excess from Stellar Winds

Cool evolved stars have ionized or partially ionized outflows which emit an excess of continuum emission at long wavelengths. This flux excess is due to thermal free-free emission and is measured relative to the expected photospheric radio flux. If the atmosphere only consisted of a static homogeneous isothermal chromosphere then the radio spectrum would be the summation of the Rayleigh-Jeans tail of the Planck function from the photosphere and the H II spectrum discussed in the previous section. At long wavelengths then, this spectrum would again have a power law of slope $F_\nu \propto \nu^2$. Cool evolved stellar atmospheres cannot in general be described by this simple model because they possess stellar winds which are escaping the gravitational potential of the star. The atmospheric density thus varies with distance from the star. In this section we briefly outline a simple analytical model for the centimeter radio flux for a star with a isothermal, constant velocity and ionization fraction wind. In Chapter **??** we relax some of these assumptions about the atmosphere's properties to derive a more complete description of the centimeter radio spectrum for these stars.

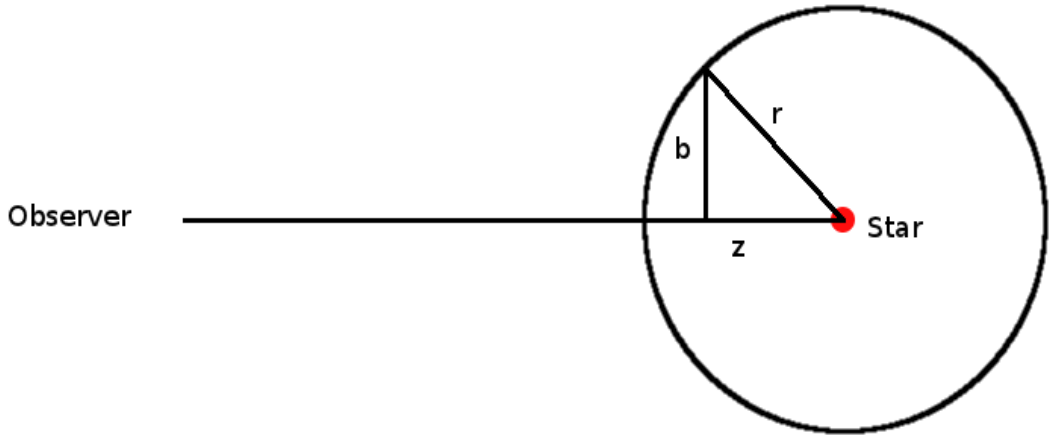

Figure 1.9: In spherical geometry the observer integrates along a ray path in the z direction, with impact parameter b, to calculate the total optical depth τ_ν, at a frequency ν.

To calculate the optical depth, we assume spherical geometry and integrate

along a ray in the z direction with impact parameter b, as shown in Figure 1.9. The total optical depth at a frequency ν is then

$$\tau_\nu = \int_{-\infty}^{\infty} \kappa_\nu dz \tag{1.49}$$

where the opacity is defined in Equation 1.45. For a constant velocity the electron density is just $n_e(r) = n_e(r_0)^2(r_0/r)^2$ and so the optical depth can be written as

$$\tau_\nu = \frac{0.212 n_e(r_0)^2 r_0^4}{T^{1.35}\nu^{2.1}} \int_{\infty}^{\infty} \frac{dz}{(b^2+z^2)^2} \tag{1.50}$$

The solution to this integral is given by

$$\int_{-\infty}^{\infty} \frac{dz}{(b^2+z^2)^{A/2}} = b^{1-A}\sqrt{\pi}\frac{\Gamma(A/2-1/2)}{\Gamma(A/2)} \tag{1.51}$$

and so the total optical depth along a ray with impact parameter b is:

$$\tau_\nu = \frac{C}{b^3} \qquad \text{where} \quad C = \frac{0.333 n_e(r_0)^2 r_0^4}{T^{1.35}\nu^{2.1}} \tag{1.52}$$

To calculate the flux density we use Equation 1.37 and assume that the source function is given by the Planck function in the Rayleigh-Jeans approximation:

$$F_\nu = \frac{2\pi}{d^2}\frac{2\nu^2 kT}{c^2}\int_0^{\infty}(1-e^{-C/b^3})bdb \tag{1.53}$$

This integral can be solved using the following expression

$$\int_0^{\infty} y^{v-1}(1-e^{-uy^p})dy = \frac{-1}{|p|}u^{-v/p}\Gamma\left(\frac{v}{p}\right), \tag{1.54}$$

which is given in Gradshteyn & Ryzhik (1994). The solution to our integral is then $1.3395C^{2/3}$ and so the total flux density can be written as

$$F_\nu = 2.574\frac{\pi k}{c^2}\frac{n_e(r_0)^{4/3} r_0^{8/3} T^{0.1}\nu^{0.6}}{d^2}. \tag{1.55}$$

Substituting in the mass continuity equation gives

$$F_\nu = 0.277\frac{k}{\mu^{4/3}c^2 m_{\rm H}^{4/3}}\frac{\dot{M}^{4/3}T^{0.1}\nu^{0.6}}{v^{4/3}d^2}. \tag{1.56}$$

where μ is the mean atomic weight of the gas and $m_{\rm H}$ is the mass of a hydrogen atom. This equation shows that the expected spectral index for an isothermal constant velocity and ionization fraction stellar outflow (i.e., a constant property wind) is $\alpha = 0.6$. Equation 1.56 is equivalent to Equation 24 in Panagia & Felli (1975).

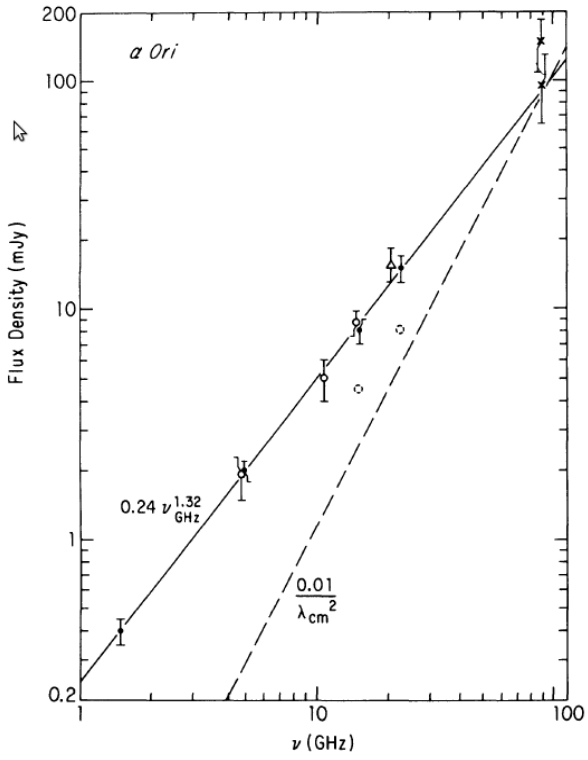

Figure 1.10: Example of a cool evolved star's radio flux excess, which is a direct result of their ionized atmospheres. Here, multi-wavelength radio observation of Betelgeuse are plotted along with a best fit power law indicating a spectral index of $\alpha = 1.32$ (Newell & Hjellming, 1982). Even though the observed flux density decreases at longer wavelengths, the excess increases relative to the expected photospheric flux (dashed line).

The free-free emission from evolved cool stars is weak (usually less than 1 mJy at $\lambda > 3$ cm) and therefore only a handful of these stars have known radio spectral indices at long wavelengths. The small number of such stars whose spectral indices are known have values which are greater than 0.6 (e.g. Drake & Linsky,

1986) due the assumptions in the constant property wind model being too simplistic. Betelgeuse is by far the best studied evolved cool star at radio wavelengths and its radio spectrum is shown in Figure 1.10 (Newell & Hjellming, 1982). Its spectral index clearly deviates from 0.6. In Chapter **??** we derive a new version of Equation 1.55 which accounts for a thermal gradient in the outflow along with flow acceleration. Nevertheless, Figure 1.10 is a good example of the radio flux excess which is present for all all cool evolved. Even though the observed flux density decreases to longer wavelengths, the excess increases relative to the expected photospheric flux as clearly seen in Figure 1.10.

1.8.5 Molecular Emission Lines from Stellar Winds

The large mass-loss rates of red supergiants along with their low outflow velocities, results in relatively high density winds. This means that these winds are very extended compared to the size of the star itself. The low temperature regime ($T < 1000\,K$) of the outer winds (i.e., the CSE) favour the formation of molecules whose emission line profiles have traditionally been studied with single dish radio antennas. As shown in Figure 1.11, these line profiles are generally either flat topped, if the lines are optically thin, or parabolic, if the lines are optically thick. These profile shapes are based on the assumption that the radio antenna is unable to spatially resolve the CSE, which has traditionally been common due to the low resolution of single dish radio antennas. If however, the antenna has the capability to resolve the CSE, then the optically thin line profiles become horned shaped and the optically thick line profiles become less parabolic, as shown in Figure 1.11. This is due to the fact the radio antenna does not detect the most extended emission, which has the lowest absolute velocities, and therefore the flux density at the center of the line profile is lower than the rest of the line in the optically thin case.

If these molecular line profiles are observed with a radio interferometer, the appearance of the line can be the same as in Figure 1.11, but the reasons will be different. To explain these reasons, we concentrate on an optically thin emission line. If the emission is unresolved by the interferometer, then as before the profile will be flat topped. However, if the emission is resolved by the interferometer then

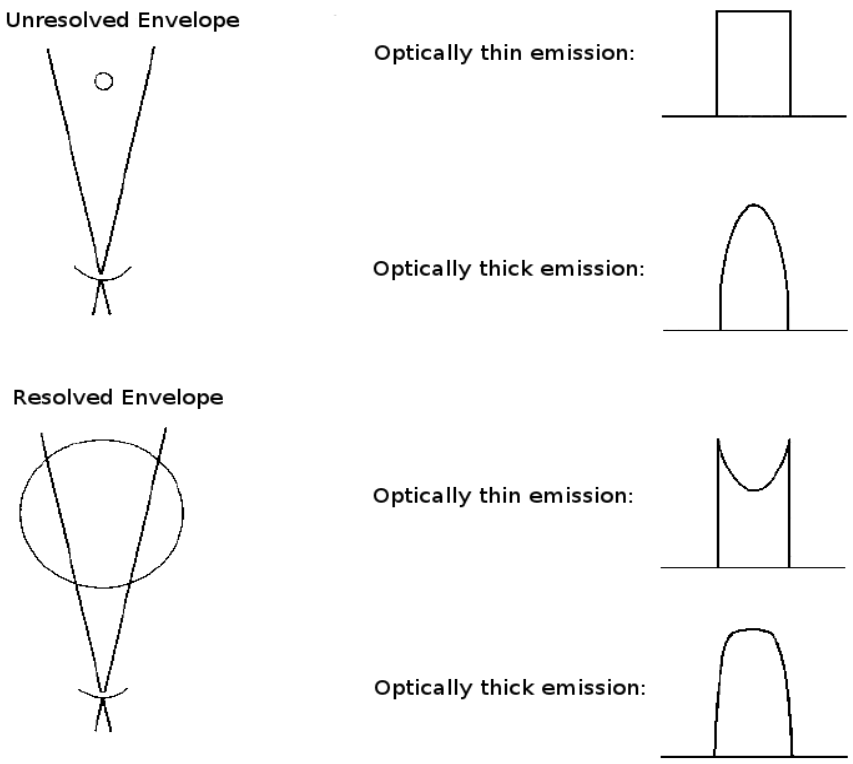

Figure 1.11: Theoretical molecular line profiles of a CSE from a single dish radio antenna. Unresolved line profiles are flat topped for optically thin emission and parabolic for optically thick emission. If the CSE is spatially resolved, the optically thin profile becomes a *horned shaped* line while the optically thick line becomes less parabolic. Figure adapted from Dalgarno & Layzer (1987).

the profile may take on two different appearances, depending on the *resolving-out scale*[1] of the interferometer. If the emission occurs on scales that are less then the interferometer's resolving-out scale then all emission is recovered and the profile will just have a flat topped appearance. However, if the emission is extended on scales larger then the resolving-out scale, then the interferometer will not detect the material at low absolute velocities (i.e., the most extended material) and the profile will have a horned-shaped appearance.

Molecular emission lines from red supergiants generally have lines widths of the order $20 \rightarrow 50\,\mathrm{km\,s^{-1}}$, indicative of $10 \rightarrow 25\,\mathrm{km\,s^{-1}}$outflows. Even though

[1] An interferometer cannot not recover emission on scales larger than this. See Chapter **??**.

these velocities are lower than the photospheric escape velocity (generally of the order $50 \rightarrow 100\,\mathrm{km\,s^{-1}}$), these molecular emission lines are formed in the CSE where the escape velocity is much lower than at the photosphere and so these lines are indicative of mass-loss.

The most important molecule used in the study red supergiant outflows is CO as it can be observed in both O-rich and C-rich stars. CO is a very stable molecule and can form in the photospheres of very cool stars and persist far out into the CSE. In typical CSE conditions, the rotational levels in CO are excited via collisions with H_2 molecules and photo-excitation of the vibrational levels by IR photons in a process known as *infrared pumping* (Lamers & Cassinelli, 1999). It is the de-excitation of the rotational transitions of $v = 0$ which produce emission lines at radio (i.e., mm) wavelengths. If collisions are the dominant means of populating the rotational levels (i.e., collisions are more important than infrared pumping) then the distribution of the molecules over the J levels will be approximately in local thermodynamic equilibrium (LTE) with respect to the gas temperature. If however, infrared pumping is the most efficient means of populating the levels, then the distribution will deviate from LTE.

1.9 Outline and Goals of this Thesis

A

List of Abbreviations Used in this Thesis.

Table A.1: List of Abbreviations

Acronym	Meaning
ALMA	The Atacama Large Millimeter/submillimeter Array
AGB	Asymptotic Giant Branch
BIMA	Berkeley Illinois Maryland Association
CARMA	Combined Array for Research in Millimeter-wave Astronomy
CSE	Circumstellar Envelope
DDT	Director's Discretionary Time
e-MERLIN	e-Multi-Element Radio Linked Interferometer Network
FOV	Field of View
GHRS	Goddard High-Resolution Spectrograph
GREAT	German Receiver for Astronomy at Terahertz Frequencies
HPBW	Half Power Beamwidth
H-R	Hertzsprung-Russell
HST	Hubble Space Telescope
IOTA	Infrared Optical Telescope Array
IR	Infrared
IRAM	Institut de Radioastronomie Millimétrique
IUE	International Ultraviolet Explorer
LSR	Local Standard of Rest

Continued on next page

Table A.1 – *Continued from previous page*

Acronym	**Meaning**
LTE	Local Thermodynamic Equilibrium
MEM	Maximum Entropy Method
MHD	Magnetohydrodynamic
OVRO	Owens Valley Radio Observatory
OSRO	Open Shared Risk Observing
RF	Radio Frequency
RFI	Radio Frequency Interference
RGC	Red Giant Clump
RGB	Red Giant Branch
RSG	Red Supergiant
S/N	signal-to-noise ratio
SGB	Subgiant Branch
SOFIA	Stratospheric Observatory for Infrared Astronomy
SMA	Submillimeter Array
SZA	Sunyaev-Zel'dovich Array
SIS	superconductorinsulatorsuperconductor
UV	Ultraviolet
VLA	Karl G. Jansky Very Large Array
VLBA	Very Long Baseline Array
VLT	Very Large Telescope
W-R	Wolf-Rayet

B

Discrete Absorption Feature

The temperature equation outlined in Chapter **??** assumes that the wind is homogenous, but this may not be the case for Arcturus. During this study we analyzed STIS spectra of Arcturus from the online StarCAT catalog (Ayres, 2010b). The Mg II h and k lines from data obtained in 2001 show a wind velocity $\sim 30 - 40$ km s^{-1}, which is similar to that adopted in the Drake models for this star Drake (1985). A narrow discrete absorption feature is found at -49 km s^{-1} in the broad blue-shifted wind absorption component of both lines as shown in Figure B.1. For this discrete feature we find a most probable turbulent velocity of 3.4 km s^{-1} and a Mg column density[1] of 1.4×10^{12} cm^{-2}. A Mg column density of 10^{15} cm^{-2} is required to produce the blueward absorption components in the h and k lines (McClintock *et al.*, 1978). Therefore, this discrete absorption feature accounts for $\sim 0.1\%$ of the total wind column density.

[1] Assuming all Mg to be Mg II

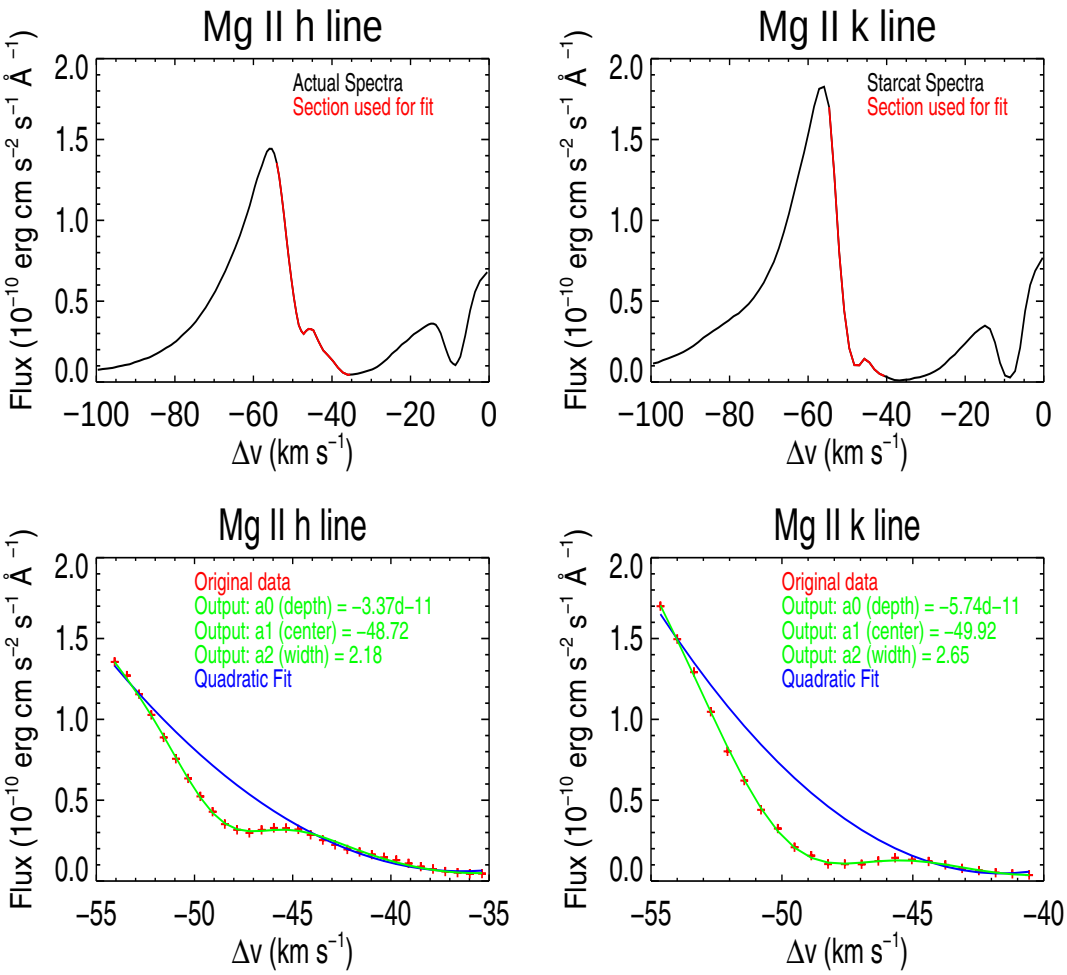

Figure B.1: Analysis on the absorption feature found in the Mg II h and k lines. A function composed of a linear combination of a Gaussian and a quadratic fitted the discrete absorption feature the best. The red data in the upper row shows the data that is used in this analysis.

References

Adams, W.S. & MacCormack, E. (1935). Systematic Displacements of Lines in the Spectra of Certain Bright Stars. *Astrophysical Journal*, **81**, 119. (Cited on page 4.)

Altenhoff, W.J., Mezger, P.G., Wendker, H.J. & Westerhout, G. (1960). Veröff. Sternwärte, Bonn. **59**, 48. (Cited on page 30.)

Ayres, T. (2010a). A stellar perspective on chromospheres. *Memorie della Societa Astronomia Italiana*, **81**, 553. (Cited on page 7.)

Ayres, T.R. (2010b). StarCAT: A Catalog of Space Telescope Imaging Spectrograph Ultraviolet Echelle Spectra of Stars. *Astrophysical Journal Supplemental Series*, **187**, 149–171. (Cited on page 40.)

Ayres, T.R., Linsky, J.L., Vaiana, G.S., Golub, L. & Rosner, R. (1981). The cool half of the H-R diagram in soft X-rays. *Astrophysical Journal*, **250**, 293–299. (Cited on pages 2 and 5.)

Ayres, T.R., Brown, A., Harper, G.M., Bennett, P.D., Linsky, J.L., Carpenter, K.G. & Robinson, R.D. (1997). Digging Deeper in the Coronal Graveyard. *Astrophysical Journal*, **491**, 876. (Cited on page 5.)

Beck, P.G., Bedding, T.R., Mosser, B., Stello, D., Garcia, R.A., Kallinger, T., Hekker, S., Elsworth, Y., Frandsen, S., Carrier, F., De Ridder, J., Aerts, C., White, T.R., Huber, D., Dupret, M.A., Montalbán, J., Miglio, A., Noels, A., Chaplin, W.J., Kjeldsen, H., Christensen-Dalsgaard, J., Gilliland, R.L., Brown, T.M., Kawaler, S.D., Mathur, S. & Jenkins, J.M. (2011). Kepler Detected Gravity-Mode Period Spacings in a Red Giant Star. *Science*, **332**, 205–. (Cited on page 20.)

Bedding, T.R., Mosser, B., Huber, D., Montalbán, J., Beck, P., Christensen-Dalsgaard, J., Elsworth, Y.P., García, R.A., Miglio, A., Stello, D., White, T.R., De Ridder, J., Hekker, S., Aerts, C., Barban, C., Belkacem, K., Broomhall, A.M., Brown, T.M., Buzasi, D.L., Carrier, F., Chaplin, W.J., di Mauro, M.P., Dupret, M.A., Frandsen, S., Gilliland, R.L., Goupil, M.J., Jenkins, J.M., Kallinger, T., Kawaler, S., Kjeldsen, H., Mathur, S., Noels, A., Aguirre, S.V. & Ventura, P. (2011). Gravity modes as a way to distinguish between hydrogen- and helium-burning red giant stars. *Nature*, **471**, 608–611. (Cited on page 20.)

Berio, P., Merle, T., Thévenin, F., Bonneau, D., Mourard, D., Chesneau, O., Delaa, O., Ligi, R., Nardetto, N., Perraut, K., Pichon, B., Stee, P., Tallon-Bosc, I., Clausse, J.M., Spang, A., McAlister, H., ten Brummelaar, T., Sturmann, J.,

Sturmann, L., Turner, N., Farrington, C. & Goldfinger, P.J. (2011). Chromosphere of K giant stars. Geometrical extent and spatial structure detection. *Astronomy & Astrophysics*, **535**, A59. (Cited on page 7.)

Bernat, A.P. & Lambert, D.L. (1976). K I 7699 A emission from the Betelgeuse shell. *Astrophysical Journal*, **210**, 395–401. (Cited on page 4.)

Carpenter, K.G., Brown, A. & Stencel, R.E. (1985). The geometric extent of C II (UV 0.01) emitting regions around luminous, late-type stars. *Astrophysical Journal*, **289**, 676–680. (Cited on page 7.)

Carpenter, K.G., Robinson, R.D., Harper, G.M., Bennett, P.D., Brown, A. & Mullan, D.J. (1999). GHRS Observations of Cool, Low-Gravity Stars. V. The Outer Atmosphere and Wind of the Nearby K Supergiant lambda Velorum. *Astrophysical Journal*, **521**, 382–406. (Cited on page 6.)

Castor, J.I., Abbott, D.C. & Klein, R.I. (1975). Radiation-driven winds in Of stars. *Astrophysical Journal*, **195**, 157–174. (Cited on page 12.)

Chapman, S. & Zirin, H. (1957). Notes on the Solar Corona and the Terrestrial Ionosphere. *Smithsonian Contributions to Astrophysics*, **2**, 1. (Cited on page 12.)

Chiosi, C. & Maeder, A. (1986). The evolution of massive stars with mass loss. *Annual Review of Astronomy & Astrophysics*, **24**, 329–375. (Cited on page 2.)

Cranmer, S.R. & Saar, S.H. (2011). Testing a Predictive Theoretical Model for the Mass Loss Rates of Cool Stars. *Astrophysical Journal*, **741**, 54. (Cited on page 13.)

Crowley, C., Espey, B.R., Harper, G.M. & Roche, J. (2009). Winds and Chromospheres of Cool (Super-) Giants. In E. Stempels, ed., *15th Cambridge Workshop on Cool Stars, Stellar Systems, and the Sun*, vol. 1094 of *American Institute of Physics Conference Series*, 267–274. (Cited on pages 2 and 3.)

Dalgarno, A. & Layzer, D. (1987). *Spectroscopy of Astrophysical Plasmas*. (Cited on page 36.)

Danchi, W.C., Bester, M., Degiacomi, C.G., Greenhill, L.J. & Townes, C.H. (1994). Characteristics of dust shells around 13 late-type stars. *Astronomical Journal*, **107**, 1469–1513. (Cited on page 14.)

Deutsch, A.J. (1956). The Circumstellar Envelope of Alpha Herculis. *Astrophysical Journal*, **123**, 210. (Cited on page 4.)

Dohm-Palmer, R.C. & Skillman, E.D. (2002). The Ratio of Blue to Red Supergiants in Sextans A from Hubble Space Telescope Imaging. *Astronomical Journal*, **123**, 1433–1437. (Cited on page 2.)

Draine, B.T. (2011). *Physics of the Interstellar and Intergalactic Medium*. (Cited on page 25.)

Drake, S. & Linsky, J. (1986). Radio continuum emission from winds, chromospheres, and coronae of cool giants and supergiants. *Astronomical Journal*, **91**, 602–620. (Cited on pages 5, 13 and 34.)

Drake, S.A. (1985). Modeling lines formed in the expanding chromospheres of red giants. In J.E. Beckman & L. Crivellari, eds., *Progress in stellar spectral line formation theory; Proceedings of the Advanced Research Workshop, Trieste, Italy, September 4-7, 1984 (A86-37976 17-90). Dordrecht, D. Reidel Publishing Co., 1985, p. 351-357.*, 351–357. (Cited on page 40.)

Dulk, G.A. (1985). Radio emission from the sun and stars. *Annual Review of Astronomy & Astrophysics*, **23**, 169–224. (Cited on page 23.)

Dupree, A.K., Lobel, A., Young, P.R., Ake, T.B., Linsky, J.L. & Redfield, S. (2005). A Far-Ultraviolet Spectroscopic Survey of Luminous Cool Stars. *Astrophysical Journal*, **622**, 629–652. (Cited on page 5.)

Eaton, J.A. (2008). A Model for the Chromosphere/Wind of 31 Cygni and Its Implications for Single Stars. *Astronomical Journal*, **136**, 1964–1979. (Cited on page 3.)

Falceta-Gonçalves, D., Vidotto, A.A. & Jatenco-Pereira, V. (2006). On the magnetic structure and wind parameter profiles of Alfvén wave driven winds in late-type supergiant stars. *Monthly Notices of the Royal Astronomical Society*, **368**, 1145–1150. (Cited on page 3.)

Gehrz, R.D. & Woolf, N.J. (1971). Mass Loss from M Stars. *Astrophysical Journal*, **165**, 285. (Cited on pages 4 and 14.)

Gradshteyn, I.S. & Ryzhik, I.M. (1994). *Table of integrals, series and products*. (Cited on page 33.)

Habing, H.J. (1996). Circumstellar envelopes and Asymptotic Giant Branch stars. *Astronomy & Astrophysics Review*, **7**, 97–207. (Cited on page 13.)

Haisch, B.M., Linsky, J.L. & Basri, G.S. (1980). Outer atmospheres of cool stars. IV - A discussion of cool stellar wind models. *Astrophysical Journal*, **235**, 519–533. (Cited on page 2.)

Harper, G.M. (1988). *The outer atmospheres of hybrid giants*. Ph.D. thesis, Oxford Univ. (England). (Cited on page 2.)

Harper, G.M. (2010). Betelgeuse: A Case Study of an Inhomogeneous Extended Atmosphere. In C. Leitherer, P.D. Bennett, P.W. Morris & J.T. Van Loon, eds., *Hot and Cool: Bridging Gaps in Massive Star Evolution*, vol. 425 of *Astronomical Society of the Pacific Conference Series*, 152. (Cited on page 3.)

Harper, G.M., Brown, A. & Lim, J. (2001). A Spatially Resolved, Semiempirical Model for the Extended Atmosphere of α Orionis (M2 Iab). *Astrophysical Journal*, **551**, 1073–1098. (Cited on pages 2, 7 and 14.)

Hartmann, L. & Avrett, E.H. (1984). On the extended chromosphere of Alpha Orionis. *Astrophysical Journal*, **284**, 238–249. (Cited on page 14.)

Hartmann, L. & MacGregor, K.B. (1980). Momentum and energy deposition in late-type stellar atmospheres and winds. *Astrophysical Journal*, **242**, 260–282. (Cited on pages 2 and 14.)

Hollweg, J.V. (1973). ALFVtN Waves in a Two-Fluid Model of the Solar Wind. *Astrophysical Journal*, **181**, 547–566. (Cited on page 13.)

Holzer, T.E. & MacGregor, K.B. (1985). Mass loss mechanisms for cool, low-gravity stars. In M. Morris & B. Zuckerman, eds., *Mass Loss from Red Giants*, vol. 117 of *Astrophysics and Space Science Library*, 229–255. (Cited on page 2.)

Hummer, D.G. (1988). A fast and accurate method for evaluating the nonrelativistic free-free Gaunt factor for hydrogenic ions. *Astrophysical Journal*, **327**, 477–484. (Cited on page 30.)

Iben, I., Jr. (1967). Stellar Evolution Within and off the Main Sequence. *Annual Review of Astronomy & Astrophysics*, **5**, 571. (Cited on page 18.)

Iben, I., Jr. (1993). On Why Intermediate-Mass Stars Become Giants after the Exhaustion of Hydrogen in Their Cores. *Astrophysical Journal*, **415**, 767. (Cited on page 15.)

Jones, M.H. (2008). The incidence of mid-infrared excesses in G and K giants. *Monthly Notices of the Royal Astronomical Society*, **387**, 845–855. (Cited on pages 2 and 14.)

Josselin, E. & Plez, B. (2007). Atmospheric dynamics and the mass loss process in red supergiant stars. *Astronomy & Astrophysics*, **469**, 671–680. (Cited on page 14.)

Judge, P.G. & Carpenter, K.G. (1998). On Chromospheric Heating Mechanisms of "Basal Flux" Stars. *Astrophysical Journal*, **494**, 828. (Cited on page 2.)

Karzas, W.J. & Latter, R. (1961). Electron Radiative Transitions in a Coulomb Field. *Astrophysical Journal Supplemental Series*, **6**, 167. (Cited on page 23.)

Lamers, H.J.G.L.M. (1998). Stellar Wind Theories. *Astrophysics & Space Science*, **260**, 81–100. (Cited on page 10.)

Lamers, H.J.G.L.M. & Cassinelli, J.P. (1999). *Introduction to Stellar Winds*. (Cited on pages 8 and 37.)

Levesque, E.M. (2010). The Physical Properties of Red Supergiants. In C. Leitherer, P.D. Bennett, P.W. Morris & J.T. Van Loon, eds., *Hot and Cool: Bridging Gaps in Massive Star Evolution*, vol. 425 of *Astronomical Society of the Pacific Conference Series*, 103. (Cited on page 17.)

Lim, J., Carilli, C.L., White, S.M., Beasley, A.J. & Marson, R.G. (1998). Large convection cells as the source of Betelgeuse's extended atmosphere. *Nature*, **392**, 575–577. (Cited on pages 7 and 14.)

Linsky, J.L. & Haisch, B.M. (1979). Outer atmospheres of cool stars. I - The sharp division into solar-type and non-solar-type stars. *Astrophysical Journal Letters*, **229**, L27–L32. (Cited on pages 2 and 4.)

Luttermoser, D.G., Johnson, H.R. & Eaton, J. (1994). The chromospheric structure of the cool giant star G Herculis. *Astrophysical Journal*, **422**, 351–365. (Cited on page 7.)

Macchetto, F. & Penston, M.V. (1978). The International Ultraviolet Explorer. *ESA Bulletin*, **13**, 9–14. (Cited on page 4.)

Maeder, A. & Meynet, G. (1987). Grids of evolutionary models of massive stars with mass loss and overshooting - Properties of Wolf-Rayet stars sensitive to overshooting. *Astronomy & Astrophysics*, **182**, 243–263. (Cited on page 17.)

McClintock, W., Moos, H.W., Henry, R.C., Linsky, J.L. & Barker, E.S. (1978). Ultraviolet observations of cool stars. VI - L alpha and MG II emission line profiles (and a search for flux variability) in Arcturus. *Astrophysical Journal Supplemental Series*, **37**, 223–233. (Cited on page 40.)

Morton, D.C. (1967). Mass Loss from Three OB Supergiants in Orion. *Astrophysical Journal*, **150**, 535. (Cited on page 11.)

Neugebauer, M. & Snyder, C.W. (1962). Solar Plasma Experiment. *Science*, **138**, 1095–1097. (Cited on page 13.)

Newell, R.T. & Hjellming, R.M. (1982). Radio emission from the extended chromosphere of Alpha Orionis. *Astrophysical Journal Letters*, **263**, L85–L87. (Cited on pages 34 and 35.)

Owocki, S. (2004). Stellar wind mechanisms and instabilities. In M. Heydari-Malayeri, P. Stee & J.P. Zahn, eds., *EAS Publications Series*, vol. 13 of *EAS Publications Series*, 163–250. (Cited on page 12.)

Panagia, N. & Felli, M. (1975). The spectrum of the free-free radiation from extended envelopes. *Astronomy & Astrophysics*, **39**, 1–5. (Cited on page 34.)

Parker, E.N. (1958). Dynamics of the Interplanetary Gas and Magnetic Fields. *Astrophysical Journal*, **128**, 664. (Cited on pages 12 and 13.)

Parker, E.N. (1983). Magnetic Neutral Sheets in Evolving Fields - Part Two - Formation of the Solar Corona. *Astrophysical Journal*, **264**, 642. (Cited on page 13.)

Parker, E.N. (1988). Nanoflares and the solar X-ray corona. *Astrophysical Journal*, **330**, 474–479. (Cited on page 13.)

Reimers, D. (1975). Circumstellar absorption lines and mass loss from red giants. *Memoires of the Societe Royale des Sciences de Liege*, **8**, 369–382. (Cited on page 4.)

Reimers, D. (1982). Detection of further red giants with 'hybrid' atmospheres and a possible correlation with double circumstellar MG II and CA II lines. *Astronomy & Astrophysics*, **107**, 292–299. (Cited on page 5.)

Renzini, A., Greggio, L., Ritossa, C. & Ferrario, L. (1992). Why stars inflate to and deflate from red giant dimensions. *Astrophysical Journal*, **400**, 280–303. (Cited on page 15.)

Robinson, R.D., Carpenter, K.G. & Brown, A. (1998). Goddard High-Resolution Spectrograph Observations of Cool Low-Gravity Stars. IV. A Comparison of the K5 III Stars alpha Tauri and gamma Draconis. *Astrophysical Journal*, **503**, 396. (Cited on page 7.)

Rohlfs, K. & Wilson, T.L. (1996). *Tools of Radio Astronomy*. (Cited on page 27.)

Rybicki, G.B. & Lightman, A.P. (1979). *Radiative processes in astrophysics*. (Cited on page 23.)

Schröder, K.P. & Sedlmayr, E. (2001). The galactic mass injection from cool stellar winds of the 1 to 2.5 M_{sun} stars in the solar neighbourhood. *Astronomy & Astrophysics*, **366**, 913–922. (Cited on page 2.)

Scuderi, S., Panagia, N., Stanghellini, C., Trigilio, C. & Umana, G. (1998). Radio observations of stellar winds from early type stars. *Astronomy & Astrophysics*, **332**, 251–267. (Cited on page 20.)

Simon, T., Linsky, J.L. & Stencel, R.E. (1982). On the reality of a boundary in the H-R diagram between late-type stars with and without high temperature outer atmospheres. *Astrophysical Journal*, **257**, 225–246. (Cited on page 4.)

Spitzer, L., Jr. (1939). Spectra of M Supergiant Stars. *Astrophysical Journal*, **90**, 494. (Cited on page 4.)

Stancliffe, R.J., Chieffi, A., Lattanzio, J.C. & Church, R.P. (2009). Why Do Low-Mass Stars Become Red Giants. **26**, 203–208. (Cited on page 15.)

Stothers, R. & Chin, C.W. (1969). Advanced Phases of Evolution in Massive Red Supergiants. *Astrophysical Journal*, **158**, 1039. (Cited on page 16.)

Strassmeier, K.G., Hall, D.S., Fekel, F.C. & Scheck, M. (1993). A catalog of chromospherically active binary stars (second edition). *Astronomy & Astrophysics Supplemental*, **100**, 173–225. (Cited on page 22.)

Sugimoto, D. & Fujimoto, M.Y. (2000). Why Stars Become Red Giants. *Astrophysical Journal*, **538**, 837–853. (Cited on page 15.)

Sutmann, G. & Cuntz, M. (1995). Generation of mass loss in K giants: The failure of global oscillation modes and possible implications. *Astrophysical Journal Letters*, **442**, L61–L64. (Cited on page 2.)

Suzuki, T.K. (2007). Structured Red Giant Winds with Magnetized Hot Bubbles and the Corona/Cool Wind Dividing Line. *Astrophysical Journal*, **659**, 1592–1610. (Cited on page 3.)

van Loon, J.T. (2010). The Effects of Red Supergiant Mass Loss on Supernova Ejecta and the Circumburst Medium. In C. Leitherer, P.D. Bennett, P.W. Morris & J.T. Van Loon, eds., *Hot and Cool: Bridging Gaps in Massive Star Evolution*, vol. 425 of *Astronomical Society of the Pacific Conference Series*, 279. (Cited on page 2.)

van Loon, J.T., Cioni, M.R.L., Zijlstra, A.A. & Loup, C. (2005). An empirical formula for the mass-loss rates of dust-enshrouded red supergiants and oxygen-rich Asymptotic Giant Branch stars. *Astronomy & Astrophysics*, **438**, 273–289. (Cited on page 13.)

Verdini, A. & Velli, M. (2007). Alfvén Waves and Turbulence in the Solar Atmosphere and Solar Wind. *Astrophysical Journal*, **662**, 669–676. (Cited on page 13.)

Weymann, R. (1962). Physical Conditions in the Circumstellar Envelope of α Orionis. *Astrophysical Journal*, **136**, 844–+. (Cited on page 4.)

White, S.M. (2000). The Contributions of the VLA to the Study of Radio Stars. In D.G. Finley & W.M. Goss, eds., *Radio interferometry : the saga and the science*, 86. (Cited on pages 20 and 21.)

Zuckerman, B., Kim, S.S. & Liu, T. (1995). Luminosity Class III Stars with Excess Far-Infrared Emission. *Astrophysical Journal Letters*, **446**, L79. (Cited on page 2.)